DEVELOPING A B-TAGGING ALGORITHM USING SOFT MUONS AT LEVEL-3 FOR THE DØ DETECTOR AT FERMILAB

by

Mayukh Das, B.E.

A Dissertation Presented in Partial Fulfillment
of the Requirements for the Degree of
Doctor of Philosophy

COLLEGE OF ENGINEERING AND SCIENCES
LOUISIANA TECH UNIVERSITY

MAY 2005

DEVELOPING A B-TAGGING ALGORITHM USING SOFT MUONS AT LEVEL-3 FOR THE DØ DETECTOR AT FERMILAB

by

Mayukh Das, B.E.

A Dissertation Presented in Partial Fulfillment
of the Requirements for the Degree of
Doctor of Philosophy

COLLEGE OF ENGINEERING AND SCIENCES
LOUISIANA TECH UNIVERSITY

MAY 2005

ABSTRACT

The current data-taking phase of the DØ detector at Fermilab, called Run II, is designed to aid the search for the Higgs Boson. The neutral Higgs is postulated to have a mass of 117 GeV. One of the channels promising the presence of this hypothetical particle is through the decay of b-quark into a muon. The process of identifying a b-quark in a jet using muon as a reference is b-tagging with a muon tag.

At the current data taking and analysis rate, it will take long to reach the process of identifying valid events. The triggering mechanism of the experiment, consisting of 3 levels of combined hardware, firmware and software writes final physics events at the rate of 50 Hz to data disks, with Level-3 alone accounting for the reduction from 1 kHz to 50 Hz. This large rejection is achieved through algorithms implemented in the search for key physics processes.

The work presented in this dissertation is the development of a fast b-tagging algorithm using central-matched muons, called L3FBTagMU. Additional tools such as the impact parameter tracks and calorimeter jets have been used to tag B jets. The dR or the differential increment in cone radius is the most significant variable introduced. Plots within thresholds of dR for both $Z \rightarrow bb$ Monte Carlo and monitor stream data show similar efficiency trends when checked against other parameters.

The differential efficiencies saturate at dR within 0.5 to 0.7 range. Differential bins of 0.1 intervals project an overall efficiency of tagging a b-jet in any event is 17.25 in data. This is in good agreement with the theory.

The algorithm is currently running online and offline through the DØ database repository. This work is primarily used by the b-id, B-Physics and Higgs Physics groups

for their physics analysis wherein the above b-tagging efficiency serves as a crucial tool. The prospect for optimizing the physics potential using this algorithm is very promising for current and future analyses.

DEVELOPING A B-TAGGING ALGORITHM USING SOFT MUONS AT LEVEL-3 FOR THE DØ DETECTOR AT FERMILAB

by

Mayukh Das, B.E.

A Dissertation Presented in Partial Fulfillment
of the Requirements for the Degree of
Doctor of Philosophy

COLLEGE OF ENGINEERING AND SCIENCES
LOUISIANA TECH UNIVERSITY

MAY 2005

This dissretation is dedicated to my

late Grand Parents

Shri. Mohit Kumar Das

and

Smt. Bela Rani Das

TABLE OF CONTENTS

List of Tables . . . . . **viii**

List of Figures . . . . . **ix**

Acknowledgments . . . . . **xi**

1 Introduction **1**

2 Theory **4**
2.1 Standard Model of Particle Physics 4
2.2 Higgs Mechanism and b Decay 7

3 Experimental Setup **11**
3.1 Fermilab Accelerator Assembly 11
3.2 Collisions 12
3.3 Units 14
3.3.1 Luminosity 14
3.3.2 Geometry 15
3.4 DØ Detector 15
3.4.1 Silicon Micro-strip Tracker 16
3.4.2 Central Fiber Tracker 19
3.4.3 Silicon Track Trigger 20
3.4.4 Preshower Detector 21
3.4.5 Calorimeter 22
3.4.6 Muon Detector 24
3.4.7 Trigger System and Electronics 25

4 Computing **27**
4.1 Software Framework 27
4.1.1 Packages 27
4.1.2 Interfaces 28
4.1.3 RCP 28
4.1.4 Release and Executables 28
4.2 Simulation 29
4.2.1 Event Simulation 30
4.2.2 Detector Simulation 30

4.3 Storage and Network 32

5 Design and Algorithm 33
5.1 Jet Algorithm 34
5.1.1 Jet Parameters 34
5.1.2 Locating Centers 38
5.1.3 Jet Overlap 38
5.2 Muon Algorithm 40
5.2.1 Extrapolation 41
5.2.2 Central Match 42
5.3 Track Fit 43
5.4 dR Calculation 44

6 Results and Conclusions 46
6.1 Preliminary Comparisons 46
6.2 Jets 47
6.2.1 η Distribution with All Events 47
6.2.2 η Distribution with Rejected Events 48
6.2.3 η Distribution with Accepted Events 48
6.3 Muons 51
6.3.1 η Distribution with All Events 51
6.3.2 η Distribution with Rejected Events 51
6.3.3 η Distribution with Accepted Events 54
6.4 Impact Parameter Tracks 54
6.4.1 Z0 with All Events 56
6.4.2 Z0 with Rejected Events 56
6.4.3 Z0 with Accepted Events 56
6.5 Rejection Distribution and Stringency Check 59
6.6 Efficiency 60
6.6.1 Absolute and Differential Efficiencies 61
6.7 Conclusions 63

A Code Specifics 65
A.1 The Level3.sim File Tools 65
A.2 The Level3.sim File Trigger 66
A.3 The Filter.rcp File 67

B Presentations 68
B.1 For Level-3 68
B.2 Expert Panel Reports for Silicon Track Trigger 69

Bibliography 70

LIST OF TABLES

3.1 The η position of various components of the Detector 17

6.1 Events passed by the filter hierarchy within the trigger 47
6.2 $\delta\eta$ cut against number of jets 61

LIST OF FIGURES

2.1 The Standard Model of partcle physics in its current form 5
2.2 The mass range for Higgs and respective cross-section analysis. The gluon fusion has a higher percentage of background events then the associated production modes. 8
2.3 Feynman Diagram for h→bb MC sample I 8
2.4 Feynman Diagram for the h→bb sample II 8
2.5 Different modes of decay of the b-quarks is shown in the top two diagrams. The second diagram shows how the displaced vertex or the secondary vertex is used to identify the b particle 9

3.1 The chain of accelerators at Fermilab 13
3.2 An illustration of collisions and regions 14
3.3 Mapping of η against θ 15
3.4 Run II DØ Detector 16
3.5 The SMT detector in extended form 18
3.6 Tracking system 18
3.7 Tracking done through STT 21
3.8 A transverse section of the calorimeter 23
3.9 Flow of data through triggering levels 24
3.10 The DØ trigger framework 25

4.1 Framework 28
4.2 A channeled use-case 29
4.3 Different stages of event simulation 31

5.1 An overview of the algorithm with flowchart 35
5.2 Transverse view of the jet with ϕ 36
5.3 Longitudinal view of the jet with Z and θ 36
5.4 A projected 2-3 jets in the η - ϕ plane 37
5.5 Center and centroid do not match 39
5.6 Centroid and geometric center matches 39
5.7 Split jets with two different towers 40
5.8 Central match with CFT 42
5.9 Track Parameters in X-Y Plane 44
5.10 Primary vertex location and jet reconstruction 45

6.1 Jet η distribution with all events in MC 48

6.2 Jet η distribution with all events in data 49
6.3 Jet η distribution with rejected events in MC 49
6.4 Jet η distribution with rejected events in data 50
6.5 Jet η distribution with accepted events in MC 50
6.6 Jet η distribution with accepted events in data 51
6.7 Muon η distribution with all events in MC 52
6.8 Muon η distribution with all events in monitor stream 52
6.9 Muon η distribution with rejected events in MC 53
6.10 Muon η distribution with rejected events in data 53
6.11 Muon η distribution with accepted events in MC 54
6.12 Muon η distribution with accepted events in monitor stream 55
6.13 Z0 distribution with all tracks in MC 55
6.14 Z0 distribution with all tracks in monitor stream 56
6.15 Z0 with rejected tracks in Z→bb MC 57
6.16 Z0 with rejected tracks in monitor stream 57
6.17 Z0 with accepted tracks in Z→bb MC 58
6.18 Z0 with accepted tracks in monitor stream 58
6.19 The distribution of all events against a simulated dR for acceptance and rejection 59
6.20 The check for 2 jets at dR$\leq$0.01 confirmed by 2 different towers at different η values 60
6.21 The absolute efficiency vs dR cut distribution for MC events 62
6.22 The absolute efficiency vs dR cut distribution for monitor stream data 62
6.23 The differential efficiency vs dR distribution for MC events 63
6.24 The differential efficiency vs dR distribution for monitor stream data 63

ACKNOWLEDGMENTS

When I first joined Dr. Neeti Parashar a couple of years back, I had absolutely no idea about High Energy Physics, Fermilab and the Linux environment. I am indebted to her for introducing me to this exceptionally interesting field of science. It was only through her constant support against all odds that I could accomplish my academic purpose.

I would have been a lost soul in this field without the guidance and moral support by Dr. Sudhir Malik who helped me in all steps right from my orientation to the environment to all technical and academic guidance. I am deeply thankful to Sirjee.

I am humbled at the help and guidance extended by the advisory committee and other professors in my department.

My supervisors on site at Fermilab on the DØ experiment, Dr. Rick Jesik and Dr. Per Jonsson from the Imperial College, London have always stood by my side and guided me through the technicalities of the system. They always found time to answer my questions which went a long way in finding solutions to problems.

I want to take this opportunity to thank Angela, Daniela, Claus, Stephen, Chris, Camille, Tim and everybody else in the Level-3 group at DØ who have helped me directly or indirectly in accomplishing my purpose.

I extend my special word of thanks to Lars, John, Ulrich, Tulika, Kevin, Junjie, Amitabha, David and Huishi with whom I was involved in learning and maintaining detector hardwares.

God will never forgive me if I do not mention the names of my friends who stood by me and tolerated my whims and fancies during the course of the work. I am thankful

to Anirban, Kaustubh, Anshul, Sunil, Pradip, Hemant, Jensen, Hari, Sourav, Vinay, Sankalp, Aditya, Burair, Dinker, Bimal, Alex, Jun, Anup, Bharat, Manish, Joshua, Ghalib and Sarosh.

Last but not least, a special mention of thanks to the dearest cab drivers and dispatchers at Fermilab who entertained my requests even during weird hours which nullified the disadvantage of not having a personal conveyance on site.

May I also extend my thanks to everybody whose name I have failed to mention due to negligence.

CHAPTER 1

INTRODUCTION

Human history has witnessed scientific theories of increasing power and sophistication in order to address the basic questions about the Universe. In the 18th century, Lavoisier discovered that all substances are made up of chemical elements. In the 19th century, the atom was discovered by a physicist named Dalton. The early 20th century witnessed a breakthrough discovery by Rutherford and Bohr. They found that atoms consists of dense nuclei which were orbited by electrons. In the 1930s, the nucleons or the neutron and the proton were discovered. They were considered to be elementary particles at that time. During the mid 20th century, some 300 new species of particles were discovered. They were categorized as mesons and baryons according to their texture. The confused theory started taking on some shape in the 1970s when Weinberg, Salam, Glashow and Rubbia concluded that Leptons and Quarks form the basis of elementary particles. Physicists have achieved, especially in the last 30 years, a profound understanding of the fundamental particles and the physical laws that govern matter, energy, space and time. This continuous quest has reached a defining moment. Understanding the unknown universe remains a goal with astrophysical observations. With the help of accelerator experiments, we can search for their quantum explanations. Energies at particle accelerators now match the conditions during the first instances after the big bang. It provides us with an insight of what dark matter and energy is all about. For the two ends of the exploration to

meet, it is very important that the astrophysical observations match the accelerator experiment inferences [17].

Identification of 57 different species of particles have been successfully accomplished by physicists so far. The Standard Model contains three different families of quarks, leptons, neutrinos and fundamental forces that differ in their masses. All forces in the universe can be categorized as weak, strong or electromagnetic in nature. The fundamental forces are manifestations of constituents actually governed by force carriers. The enormous variation of mass with other properties staying identical is a mysterious question. To accommodate CP-violation, the requirement of these three families stays a prerequisite for quantum physics. The main protagonist of modern day physics, Dr.Einstein, introduced the concept of unified force theory. At the most fundamental level, particles and forces may converge like a grand unification. The postulation that all forces are different manifestations of a single grand unified force theory corroborates with the possible identification of extra fields and particles [7].

The search for the minutest of particles involves the usage of energy at exceptionally higher scales. High energy particle physics concern at these exceptionally higher energy scales is limited to a very few selected places around the world. The Fermi National Accelerator lab near Chicago has the most powerful proton-anti proton collision facility available. It is designed to reach energies of the order of 1 TeV. It is the only current facility which remains in the race for the hunt of rare particles which need higher energy events. The chain of accelerators incorporated to run the Tevatron at Fermilab involves a chamber which begins by stripping a hydrogen atom of its electron till the detectors built to detect the particle shower comes out after collisions. The electronics involved in the making of the accelerators and detectors form a technology in frontier science themselves. The DØ detector consists of a complicated array of electronics and mechanical accessories equipped with the expertise to detect the rarest of particles. Chapter 3 discusses in details the accelerators and the DØ

detector. The computing system of the collaboration is as complicated and spectacular as the detector itself. The end result of algorithms go through a grueling process of data formatting, simulation, framework bugs and release certifications. Chapter 4 describes the various aspects of computing involved in the present research.

The design of the algorithm to identify b-quarks needs to be flexible. In a collaboration where a plethora of physics analysis is taking place, provision for code reusability is a matter of importance. The algorithm involves using candidates from muon, jet and track tools to check a stringently matched track within the dR threshold of a jet. The respective physics tools reference their thresholds from a master file and write results into a root tree. Additional constraint for the algorithm lies in the fact that it has to be within the timing limitation of Level-3 triggering alone.

Chapter 6 deals with the results, plots and analysis of the designed algorithm at various levels of simulation as well as real event data. For the purpose of comparison between ideal and real, Monte Carlo samples have been used. Plots for differential and absolute efficiencies have been generated and shown.

CHAPTER 2

THEORY

2.1 Standard Model of Particle Physics

Elementary particles are understood as point like constituents of matter with no known substructure up to the current limits of 10^{-18} - 10^{-19}m.

Standard Model is a mathematical framework which explains the dynamics of the elementary particles. According to this model, the fundamental constituents of matter are the fermions. The fermions are classified into leptons and quarks.

The known leptons are the electron, the muon and the tau with an electric charge of Q= -1 (in units of elementary charge e). All the three leptons have a corresponding neutrino e_ν ,μ_ν and τ_ν respectively with Q=0.

There are three families of quarks with each family consisting of 2 quarks each. The name 'quark' arises from the book Finnegan's Wake by James Joyce. The exact term was adopted by Murray Gell-Mann who received the Nobel Prize for classifying elementary particles in the year 1969. They are named u (up), d (down), c (charm), s (strange), t (top) and b (bottom) with fractional charge Q=2/3, -1/3, 2/3, -1/3, 2/3 and -1/3, respectively.

The quarks carry an additional quantum number named 'color'. The color force increases with distance at the order of 1 GeV per Fermi. By the time a free quark is present in an observable scale, the energy is far above the pair production energy for quark-anti quark pairs. Hence, the color force is instrumental in not allowing

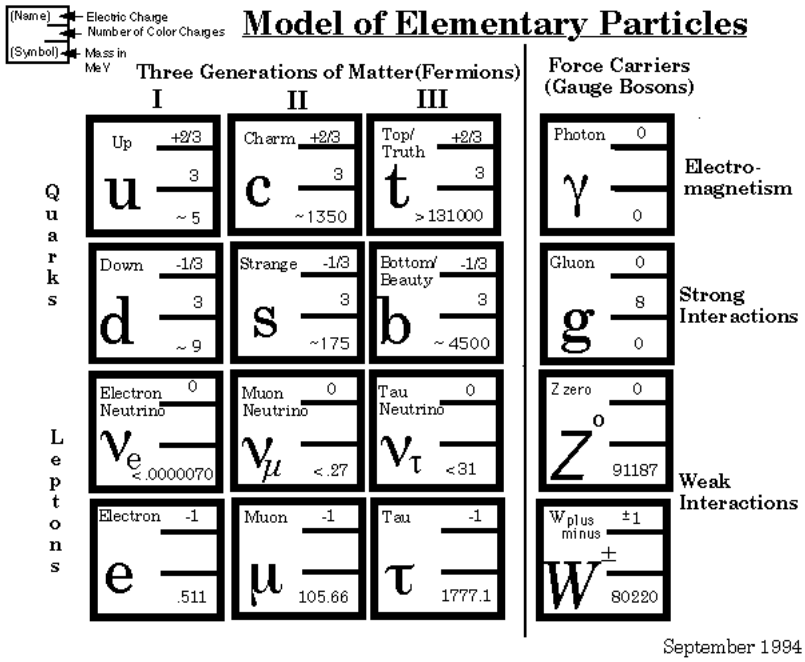

Figure 2.1: The Standard Model of partcle physics in its current form

independent existence to free quarks with the intermediate process of quark-anti quark pairs. This color can be of three different types q_i, i=1, 2, 3. Since color is not seen in nature, the elementary quarks are only seen through composite particles called baryons (combination of 3 quarks) and mesons (combination of 2 quarks). For example, the proton is a baryon composed of uud and the neutron ddu [10]. The mesons are quark and anti-quark pairs: for example, the pions, π^+ and π^-. The Standard Model also has a provision for the force carriers or the interaction particles. All force in the universe is divided into four significant categories. They are gravity, electromagnetic, strong, and weak. The reason for each of these forces is attributed to a type of force carrier or a boson. Graviton is responsible for gravity as the name suggests. The electromagnetic force carrier is photon. The strong interactions is attributed to gluons. The intermediate vector bosons $W+$, $W-$, and Z are responsible for weak interactions. Except for gravitational interaction, all the other interactions are ably accounted for in the Standard Model. The bosons have spin s=1 and interact

between fermions. Theoretically, the Standard Model is a quantum field theory based on the gauge symmetry.

$$SU(3)_c \times SU(2)_L \times U(1)_Y$$

It includes the symmetry group of the strong interaction $SU(3)_C$ and the electroweak interactions $SU(2)_L \times U(1)_Y$. The group symmetry of the electromagnetic interaction is a subgroup of the electroweak interactions.

The eight gluons form the gauge bosons for $SU(3)_C$,$W\pm$. Z and the photon are the gauge bosons of the $SU(2)_L \times U(1)_Y$. The gluons are massless and electrically neutral. The gluons are self interacting which makes their presence very interesting. The weak bosons have heavy mass and also self interact. While the $W\pm$ have charge $Q\pm$, the Z is a neutral particle. The photon is massless, charge-less and non-self interacting.

The infinite range of the electromagnetic interaction corresponds to an interaction due to a massless particle (photon). A typical range of weak interaction is about 10^{-16} cm. This is attributed to the interaction of a heavy vector boson with mass of the order of M_V ~100GeV. Although carried by massless gluons, the strong interaction has a range of 10^{-13}cm.

The electromagnetic interactions are governed by the size of the electromagnetic coupling constant e or equivalently $\alpha = \frac{e^2}{4\pi}$. At low energies it is given by fine structure constant $\frac{1}{137}$. The weak interactions happen at energies much lower than the mass of their vector bosons. The strength is given by dimension Fermi Constant GF = 1.167 x 10-5^{-2}Gev. The strong interactions strength are determined by alpha $s = \frac{gs^2}{4\pi}$. They vary from large to low values. The quarks behave as free particles when they are observed at infinitely large energies or equivalently infinitely short distances. They acquire the property of asymptotic freedom.

The Scalar Standard Model is not confirmed yet. The weak gauge bosons, being massive particles, indicate that $SU(3)_C \times SU(2)_L \times U(1)_Y$ is not a symmetry. Since the photon being massless reflects that $U(1)_em$ is a good symmetry,

$SU(3)_c \times SU(2)_L \times U(1)_Y \rightarrow SU(3)_C \times U(1)_em$ should be the symmetry breaking pattern [13]. The above pattern which is still not proved is the foundation for the Higgs mechanism to come into the picture. The discovery of the new particle, the Higgs Boson, categorically scalar and electrically neutral, has not been seen in experiments so far and remains a challenge for particle physicists worldwide.

2.2 Higgs Mechanism and b Decay

While electroweak unification was hailed as a great step forward, there remained a major conceptual problem. Since the weak and electromagnetic forces are part of the same electroweak force, still the exchange particle for the electromagnetic interaction, the photon, is massless while the W and Z have masses more than 80 times of a proton. The electromagnetic and weak forces certainly do not look the same in the present low temperature universe. Hence, there must have been some kind of spontaneous symmetry breaking as the hot universe cooled enough for particle energies to drop below 100 GeV. The theories attribute the symmetry-breaking to a field called the Higgs field, and it requires a new boson, the Higgs boson [12].

Preliminary formulation of the theory estimates that the Higgs boson would have mass energy in excess of 1 TeV. Since the discovery of the top quark, there is evidence that the Higgs boson may have energies in the range of a few hundred GeV and therefore within the range of present day accelerators. The data from the DØ detector facility is used to estimate the mass of the Higgs boson. Suggestions that it may have a mass below 200 GeV have made it one of the high priorities for high energy physics. Consistency of the Standard Model places some loose bounds on the range of the Higgs mass possible from theory. Direct searches from LEP 2 experiments places the lower limit on the Higgs at MH$\geq$114 GeV. Indirect evidence from fits to the electroweak observables points to the preferred mass of the Higgs at 135 GeV [6][12]. The two possible ways Higgs could be probed are the methods

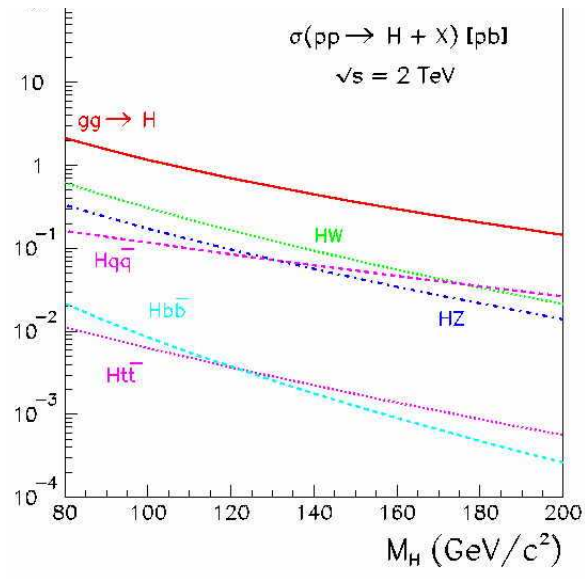

Figure 2.2: The mass range for Higgs and respective cross-section analysis. The gluon fusion has a higher percentage of background events then the associated production modes.

Figure 2.3: Feynman Diagram for h→bb MC sample I

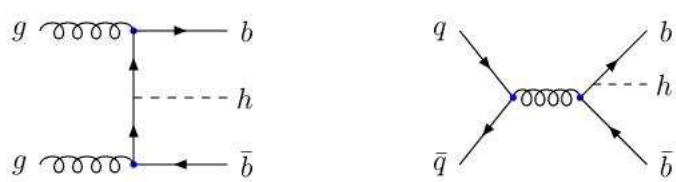

Figure 2.4: Feynman Diagram for the h→bb sample II

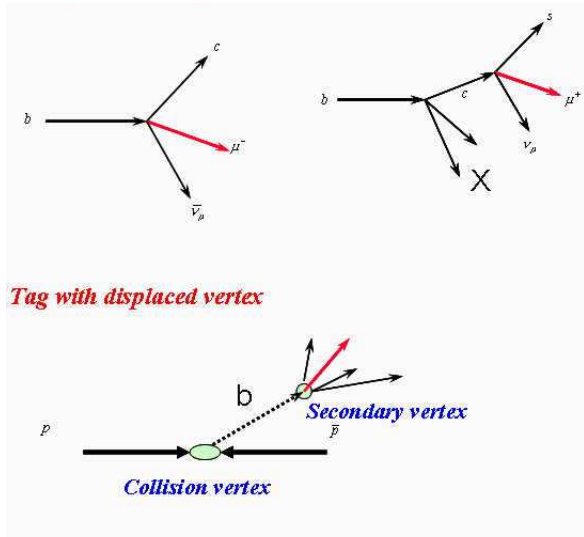

Figure 2.5: Different modes of decay of the b-quarks is shown in the top two diagrams. The second diagram shows how the displaced vertex or the secondary vertex is used to identify the b particle

of gluon fusion and the associated production. At the energy level of the Tevatron, gluon fusion is associated with a high level of background events. Hence, it becomes difficult to isolate the relevant data. On the other hand, in the associated production the most dominanat occurence is the $h \rightarrow bb$ production. The most important of these processes is the associated production of Higgs with a W and Z. The decay for these vector bosons then happen either hadronically or leptonically. The Higgs primarily decays to bottom anti-bottom quark pairs. Higgs coupling to a fermion is proportional to the squared mass of the fermion itself. Since the b-quark is three times heavier then the next heavier fermion, the efficiency for background rejection is highly improved.

The search for neutral Higgs bosons looks for a signal in the invariant mass spectrum of jets with the highest transverse energy in b-tagged multi-jet events. An ultimate number for b-tagging efficiency is the most instrumental tool desired before the Di-jet mass resolution is calculated.

To identify a jet associated with a b-quark, a technique referred to as b-tagging is performed by reconstructing the decay vertex of a long-lived B hadron within the jet. There are two main methods by which the b-quarks can be tagged. One of them is to tag the b-quarks with an impact parameter tool and the other is to tag them with a displaced vertex. The association of a soft muon tagging of b-jets is a technique with a high potential for Higgs analyses at improved efficiency for successful tagging of b-jets.

Occurence of b-quark in an event has ∼20% chance of decaying into a muon, either through a direct decay, $B \rightarrow \mu + X$, or a cascade decay,$B \rightarrow C + X, C \rightarrow \mu$. Muons from both decays are considered to be coming from a b-quark, and the jet formed by the decay products should be tagged as a B-jet [19][4].

CHAPTER 3

EXPERIMENTAL SETUP

The DØ Experiment, which is one of the two experiments placed over the Tevatron for detection of sub-atomic particles, has had a history of various runs and upgrades. While Run I took place during 1992-1995, Run II, which began in 200,1 has a goal to deliver 100 times more collisions to the experiment by the year 2009. The upgrade of the detector is also significant. The addition of a central solenoid magnetic field containing new tracking chambers is a state of the art technology being used presently.

3.1 Fermilab Accelerator Assembly

The Fermilab Tevatron, which is by far the largest collider accelerator in the world, is a 1 km long synchrotron made out of 1000 superconducting magnets. These magnets are able to concentrate and hold a 980 GeV beam of protons and anti-protons circulating in opposite directions. The two beams collide at the two interaction regions, where two detectors, namely, CDF and DØ have been placed. The interactions have a 3D-Gaussian shape and a width of about 30 cm along the beam axis (z direction). The transverse length is about $30\mu m$. Groups of protons and anti-protons cross every 360 ns.

The whole assembly starts at a Cockcroft-Walton chamber, where a single hydrogen atom is stripped of its electron to form a proton. Using a CRT, the particles are accelerated to an energy of 0.75 MeV, which is around 30 times that of the kinetic

energy of the electrons. The next step is the linear accelerator, or popularly known as the LINAC. It is 500 feet long and consists of RF cavities and is used to accelerate the ions to about 400 MeV. After passing through a carbon foil, the proton bunches enter the Booster. This is a circular synchrotron which accelerates the proton bunch to an energy of about 8 GeV. The accelerator assembly is shown in Figure 3.1. Also at this stage, the bunches are divided into two halves. One half is injected into the main injector to accelerate to an energy of 150 GeV. The other bunch is also processed through the main injector, but additionally they are bombarded over a nickel target. The spray of particles thus created have 15 anti-protons created from a million protons hitting the nickel target. The protons which are collected from this bunch after hitting the target are put into the Debuncher. The anti-protons collected are precious particles. They are cooled stochastically and transferred to the accumulator for storage. After around 150-200 x 10^{10} anti-protons are present in the accumulator, 36 bunches of protons are loaded into the Tevatron from the main injector at 150 GeV. After the successful injection of the protons, 4 bunches of anti-protons are also injected from the opposite direction. The Tevatron then accelerates both bunches to 980 GeV in one process. The beams are brought into focus in the collision regions. At this time a store is declared and the collisions are recorded for typically about 20 hours average time. The rate of collision is determined by the integral luminosity. This value keeps on decreasing due to decreased beam current and focus.

3.2 Collisions

The $p\bar{p}$ collisions primarily scatter particles at low angles. However, when there is interaction between the partons (quark or a gluon constituent), the scattering is termed as hard-scattering. Due to transformation of energy, the constituents are broken apart. The residual fragments keep tracing a narrow cylindrical track, parallel

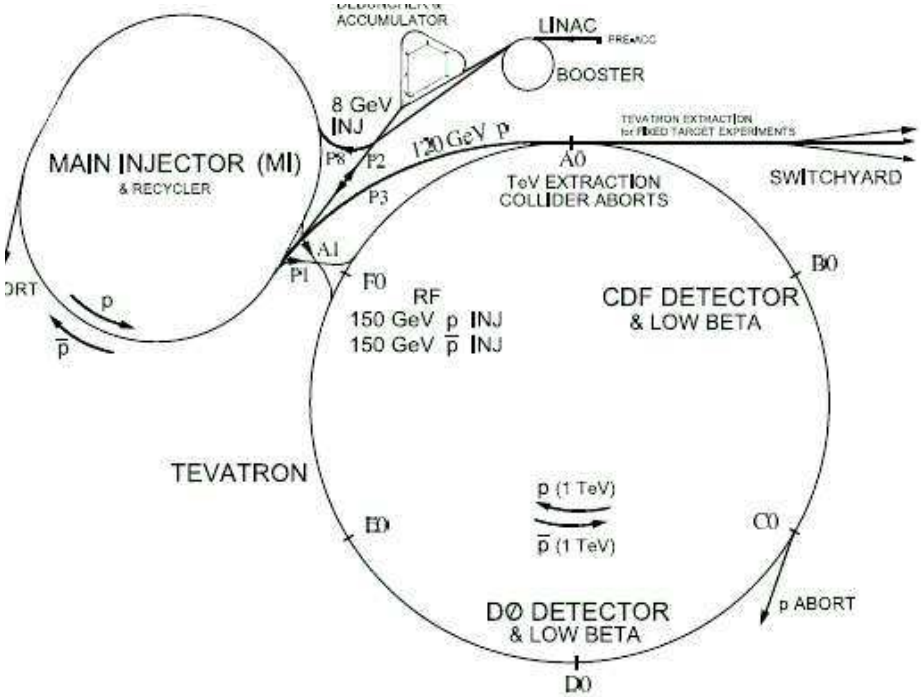

Figure 3.1: The chain of accelerators at Fermilab

to the beam-line, as small showers of color-neutral particles. The hard-scattering reaction is the possible source of intermediate resonance like the Higgs Boson. The shower of particles coming out can be any of the standard model particles. Only the leptons, neutrinos, photons and a few other strongly interacting particles like the stable hadrons leave trace and live long to reach the detectors [13]. Figure 3.2 represents collisions.

Since the electrons and muons are charged, they leave energy in the tracking detectors. The solenoid field (magnetic field in the tracking detector) bends the paths of the charged particles. The charge deposition and the bend angle helps us to determine the momentum and charge magnitude of the particle. Electrons and photons produce showers in the calorimeter where their energy is measured. Hadrons also produce showers in the calorimeter which are called jets. The toroid magnetic field, in the outer part of the detector, is used to calculate the momentum of the muon.

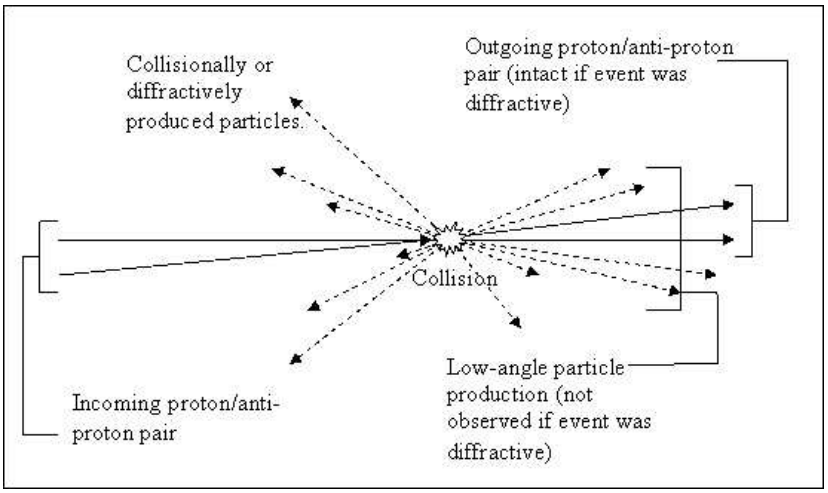

Figure 3.2: An illustration of collisions and regions

Neutrinos can be reconstructed through the conservation of total momentum. After leaving the hard-scattering region, Quarks and gluons do not live for long and undergo hadronization. It forms color-neutral particle bound states. This process creates a jet of particles traveling in the original direction of the mother particle. They are detected in the calorimeter as broad showers.

3.3 Units

3.3.1 Luminosity

Since the search for exotic rare processes are done in the experiment, a quantitative estimation is needed to figure out the rate of significant events happening in the detector. Say there is a given process N. The total number of times it happens is directly proportional to the cross-section for the event type σ and the integrated luminosity (integral with respect to the time of instantaneous luminosity) λ.

$$N = \lambda \times \sigma$$

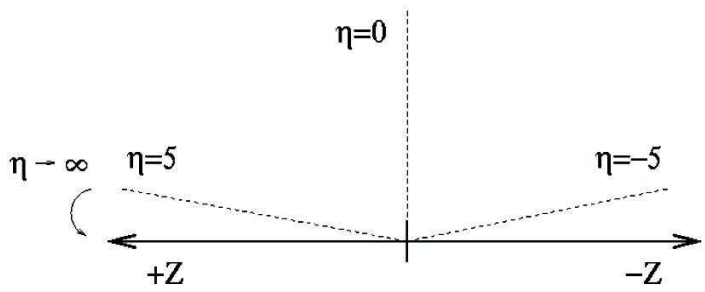

Figure 3.3: Mapping of η against θ

For a given center of mass energy, the cross-section is fixed. Hence, the goal of the accelerator remains to increase the integrated luminosity. It is $10 - 24cm^2$. The interesting physics processes happen at the cross-sections of the order of pico-barns ($10^{-36}m^2$). The integrated luminosity is calculated in inverse picobarns, pb^{-1}.

3.3.2 Geometry

Inside the detector, spherical coordinate system is used. They are r,ϕ (azimuthal angle) and θ (polar angle). The azimuthal angle is defined by the angle with respect to x-axis and the polar angle with respect to the z-axis. The center of the whole system is at the interaction region. The z-direction is the line r=0 and is defined as the beam line. Instead of θ another variable the η is used [11][9]. The DØ detector uses a right-handed coordinate system, with the origin at the center of the detector, the positive z-axis along the proton direction, and the y-axis upward. In hadron colliders, pseudorapidity, $\eta = -\ln tan\frac{\theta}{2}$, is often used since the pseudorapidity intervals are invariant under Lorentz boost. Figure 3.3 explains the mapping.

3.4 DØ Detector

The DØ detector basically consists of three main parts as shown in Figure 5.4. The inner detector contains the tracking chambers which tracks the path of the charged

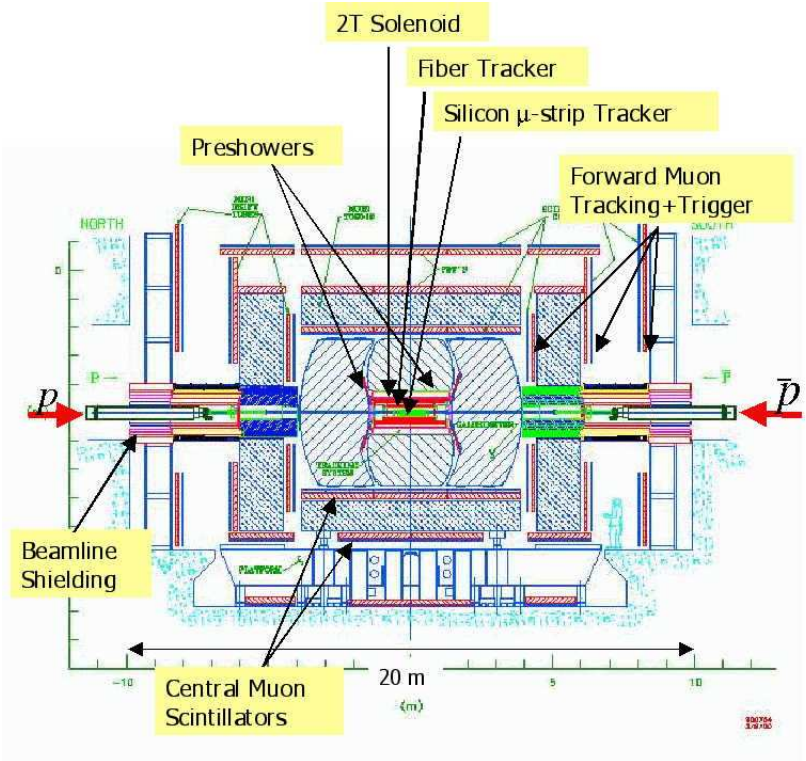

Figure 3.4: Run II DØ Detector

particles. The calorimeter, as the name suggests, is used for recording the energy deposits of the hadronic and electromagnetic particles. It surrounds the tracking detectors. The muon chambers measure the momentum of charged particles which have escaped the calorimeter and have successfully passed through the thick iron toroid magnets. The transverse energy and direction of neutrinos are calculated by following the concept of total transverse momentum conservation for each event. Lastly, a wide array of triggering and electronics with firmware is implemented to check the event rate and select significant events only.

3.4.1 Silicon Micro-strip Tracker

High resolution position measurements nearest to the interaction region for the charged particles are produced by Silicon Microstrip detector. The determination of whether tracks came from secondary vertices is a good indication of the presence of bottom

Table 3.1: The η position of various components of the Detector

Detector Information	
Detector	η Range
Luminosity Monitors	2.7 - 4.4
Silicon Microstrip Tracker	≤ 1.62
Central Fibre Tracker	≤ 1.62
Central Preshoer Detector	≤ 1.2
Forward Preshower Detector (outer)	1.4 - 1.6
Forward Preshower Detector (inner)	1.6 - 2.5
Central Calorimeter (em)	≤ 1.1
Inter-Cryostat Detector	1.1 - 1.4
End Calorimeter (em)	1.4 -2.4
Central Calorimeter (hadronic)	$\leq .7$
End Calorimeter (hadronic)	1.5 - 3.4
Inter Cryostat Detector	.7 - 1.5
Central Muon System	≤ 1.6
Forward Muon System	1.6 - 2.0

quarks. The electron-hole pairs created in the p-n junction in a silicon while the passing of charged particles is used for decision making. The pairs are separated by applying a bias voltage. The wafer slice of the silicon strips are 300 μm wide. There are additional conducting strips constructed inside the chip. They are each 50 μm wide. The charge from each strip is stored in a capacitor until it is read and digitized by special electronics. Since there is too much data to be digitized, an array of 32 capacitors hold the analog charge signal till the first layer of the trigger mechanism starts working on them. The charge is then zero-suppressed, which is a simple triggering algorithm and transferred out of the detector [5].

The detector geometry is cylindrical in nature as shown in an extended form in Figure 5.5. Six barrels surrounding the beam pipe make up the heart of the detector. Each barrel is 12 cm long and consists of 4 layers of silicon wafers and read-out chips. They are slightly overlapped in order to prevent gaps in the ϕ acceptance. Within $\eta \leq 1.1$, which is known as the central region, a single particle traverses anything

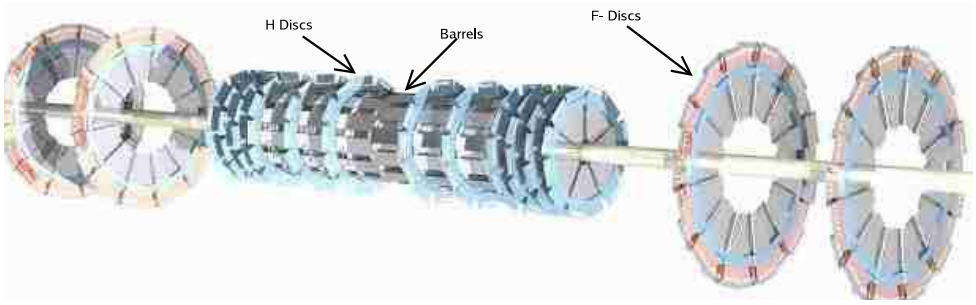

Figure 3.5: The SMT detector in extended form

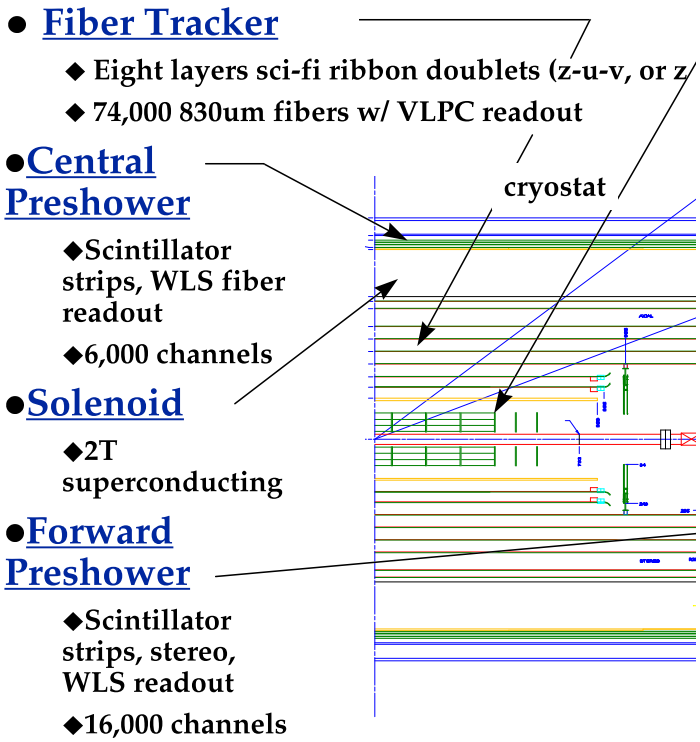

Figure 3.6: Tracking system

between 4 and 8 silicon detectors. Inefficiencies sometimes bring the number of hits down to 3 to 4.

The region between the barrels are occupied with discs placed perpendicular to the beam pipe. There are 4 disks which are placed at the end sides of the two sides of the barrels. These are known as the F-disks. They are composed of 12 F-wedges each with pixel-sized silicon detectors that extend from a radius of 2.6-10.5 cm. There are two larger H-disks placed at each end of the detector. They are made of 16 H-wedges each extending from radii of 9.5-26 cm. Together these disks extend the η coverage to 3.0.

3.4.2 Central Fiber Tracker

The silicon detector is surrounded by the Central Fiber Tracker, a detector designed to increase the efficiency of the inner tracker. The CFT detects particles up to $\eta = 2.0$. There are a total of 71,680 scintillating fibers, each containing a dye of molecules which are excited by high energy charged particles. The molecules release photons in the visible part of the electromagnetic spectrum while relaxing to the ground states which form the detection procedure.

There are a total of 8 super-layers as shown in Figure 5.6. Each super-layer is composed of two doublet-layers, an axial doublet-layer of fibers, and a stereo doublet-layer which is at a 3 degree angle relative to the beam axis. Each doublet-layer is composed of parallel, adjacent fibers bound into ribbons of 128 degrees each. The diameter of each fiber is 835μ m with a 737 μ m scintillating core. The length of the fibers ranges between 1.66m to 2.52m. A second layer is placed on top of the first, offset by half a fiber diameter. As a result, each fiber in the second layer maximally fills the space between the two fibers in the first ribbon. The efficiency of each doublet-layer is about 99% per particle including dead channels.

Wave guides are connected to each fiber at the ends carrying the photons for de-

tection. The opposite side of fibers are coated with a surface which facilitates the reflection of photons so that the particles stay in the wave guide.

An average of around 10 photons are produced by each ionizing particle hitting the detector. They are detected by a Visible Light Photon Counter (VLPC) counter. The counter converts photons into electrical signal pulses. To reduce electronic noise, the VLPC, which is a solid-state silicon device, 1 mm in diameter, operates at liquid helium temperatures. A 6V bias voltage is applied in order to create cascades of electrons from the electron-hole pairs. The cascaded electrons are detected as a current through VLPC. Quantum efficiency of about 80% and a gain of around 50,000 is obtained per photon. The photon-converted electrons are collected within a period of 100ns before the next bunch crossing takes place. There are a total of 1024 VLPCs grouped into the cassettes. The digitization and readout is done similar to that of the SMT detector [20].

3.4.3 Silicon Track Trigger

The STT is a novel device that measures the impact parameters of displaced tracks, enabling the selection of large samples of events that contain b-quarks and other long lived particles in the presence of enormous backgrounds. The STT uses the CFT track as the reference for the path extrapolated into the SMT. Silicon clusters within this path can then be included in the track fit, in addition to the original CFT information.

Central Track Trigger or the CTT is the first phase of trigger for the CFT. It accepts data from the detector's front-end and sends it to STT and the next global trigger level. CTT sends a list of up to 46 tracks to each STT crate. A 2 mm width is defined around each track as shown in Figure 3.7. Only the SMT clusters within the road are considered for track fitting. The STT uses the hits in the innermost and outermost layers of the CFT as well as clusters on three or four layers of the

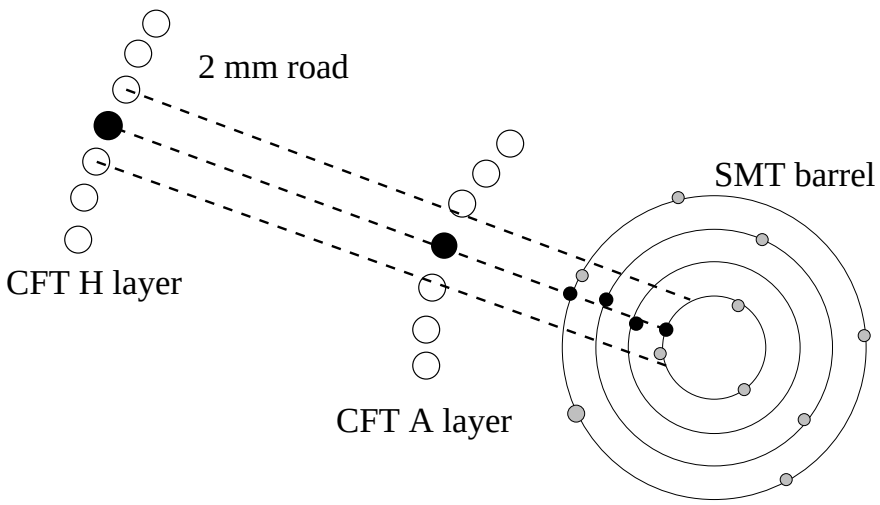

Figure 3.7: Tracking done through STT

SMT to perform the track fitting, so the STT can provide fine impact parameter resolution. The fitting result of each road is sent to the next level. Because of an overlap between sectors, most high transverse momentum tracks hit detectors that belong to the same sector in all four layers. The STT detector uses custom-designed VME boards with on-board programmable processors. Six identical crates (x70 - x75) contain the boards, serving one of the SMT sextants. Each crate has one crate controller, one Single Board Computer, one Fiber Road Card, nine Silicon Trigger Cards, and two Track Fitting Cards. Since these cards share common requirements for internal and external interfaces, they use a common motherboard, with the specific logic contained on daughter boards [8].

3.4.4 Preshower Detector

Unwanted degradation of the energy resolution happens in the electromagnetic section of the calorimeter due to the presence of the solenoid. Sampling of particle showers is needed in order to make up for the loss of energy. Preshower detectors are a pair of scintillating detectors divided into central preshower and forward preshower detectors.

The Central Preshower consists of a 6 mm lead absorber placed in front of the scintillating fibers. This increases the showering of electrons and photons. Three layers of strips of triangular cross-section constitute the whole setup. Every strip has a hole in the center with a wavelength-shifting fiber to direct light to the waveguides. The transmission of light through the VLPC is done just like it is done in the CFT.

The FPS (Forward Preshower Detector) also has the same design. It is mounted over two pieces over the calorimeter endcaps. The lead absorber plates presented here are 11 mm in thickness. The two scintillating layers lie on either side of the absorber plate. The two layers have dual roles. While the inner one detects ionized particles like the muons, the outer layer detects electromagnetic showers which get initiated in the lead plate. The inner layers are optimized to detect relatively smaller signals as compared to the outer layer. A decision is taken over the identity of the particle after comparing the outcome of both the layers during the same event. A shower initiatinga particle without a scintillating layer hit is definitely a photon while a particle which initiates scintillation in the inner layer is definitely an electron. Hence, this detector is a good measure for discriminating between photons and electrons before they reach the calorimeter.

3.4.5 Calorimeter

The calorimeter is present outside the solenoid magnet. This is the part of the detector which has a very low magnetic field. The prime purpose of this detector is to measure the energy of photons, electrons and hadronic jets of particles. The dense material of the calorimeter produces a shower of particles. These showers are sampled at various points in order to determine its shape and energy. The central calorimeter extends to $\eta \leq 1.1$. The forward regions extend to $\eta \sim 4.0$. The region between the central and forward regions, called the Inter-Cryostat Region (ICR), is covered by special detectors.

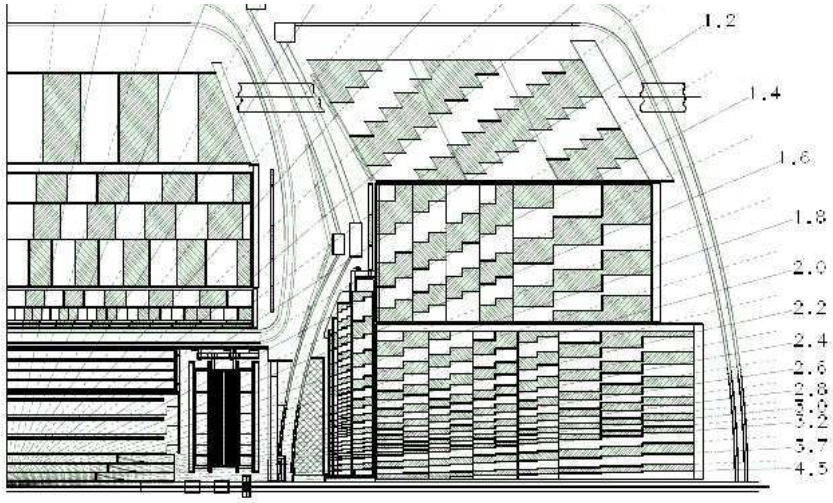

Figure 3.8: A transverse section of the calorimeter

The showers are induced due to the presence of depleted uranium. Since uranium creates the same ionization per unit length from an incoming electron or pion, it is an ideal material for the job. The resultant showers hold energies in the same region for both electromagnetic and hadronic particles. Cells that are 2.3 mm wide inside liquid argon measure the ionization created by the showers. A copper read-out pad in each cell is held at high voltage to create an anode which collects the ionization. With pad being insulated by a thick G10 coating, the ionization creates an inverse image charge which builds up the read-out pad.

The sampled charge on each pad is fed into a baseline subtracter (BLS). These BLS boards isolate the signal from the current beam-crossing from that of the previous. The ionization takes a few μs to be completely absorbed, given the 430 ns drift time in argon, as compared to 396 ns between beam crossing. If a section view of the calorimeter is taken, it will be seen that it consists of three layers. They are the electromagnetic (inner), fine hadronic, and the coarse hadronic layer (outer most) layers. The electromagnetic layers have 65.6 mm total thickness of uranium. This consists of more than 20 electromagnetic interaction average lengths. The geometry of the calorimeter is calculated in the $\eta - \phi$ plane. The first 3 layers of cells are $\eta \times \phi$

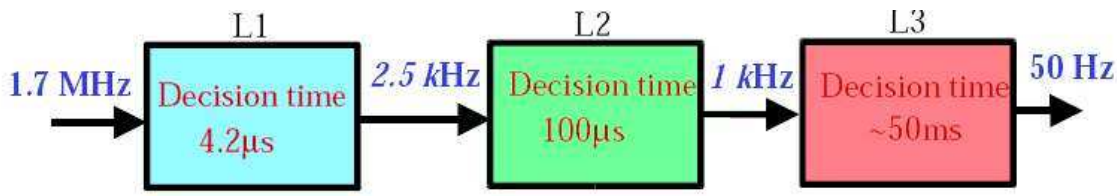

Figure 3.9: Flow of data through triggering levels

= 0.1 x 0.1 in size. The third layer, which encounters the maximum average showe,r has a granularity of the order of 0.05 x 0.05 in the same plane in the central region as shown in Figure 3.8. The fine hadronic layers have 3 layers of cells in the central regions and 4 in the forward regions. They have an identical cell size as that of the electromagnetic region. Since the coarse hadronic layer is farthest away from the center of the detector, the granularity is of the order of 0.2 x 0.2. The two hadronic layers make up around 6.4 hadronic interaction lengths, which satisfies the need for all the possible hadronic interaction regions.

The cells are arranged in a projective geometry in the $\eta \times \phi$ plane. Each $\eta \times \phi$ of 0.2 x 0.2 region are collectively called a tower. The total E_T in each tower is used for the calorimeter energy calculations [13].

3.4.6 Muon Detector

The muon detector forms the outer-most layer of the detector assembly and consists of three sub-structures or layers, namely the A, B, and C layer detectors, which are (due to the detector size) spread far apart. These structures are able to detect pasing muons using drift tubes and scintillating fibers. The drift tubes signal the passae of muons by producing detectable electron avalanches and are arranged in such a way as to facilitate the tracing of the muon's path through them. With information about the muon's path, it's momentum can be determined. Muons carrying high energy with a transverse momentum of 3 GeV are measured in the muon detectors. A 2000 ton, 1.9 Tesla iron toroid magnet bends the paths of the muons and absorbs

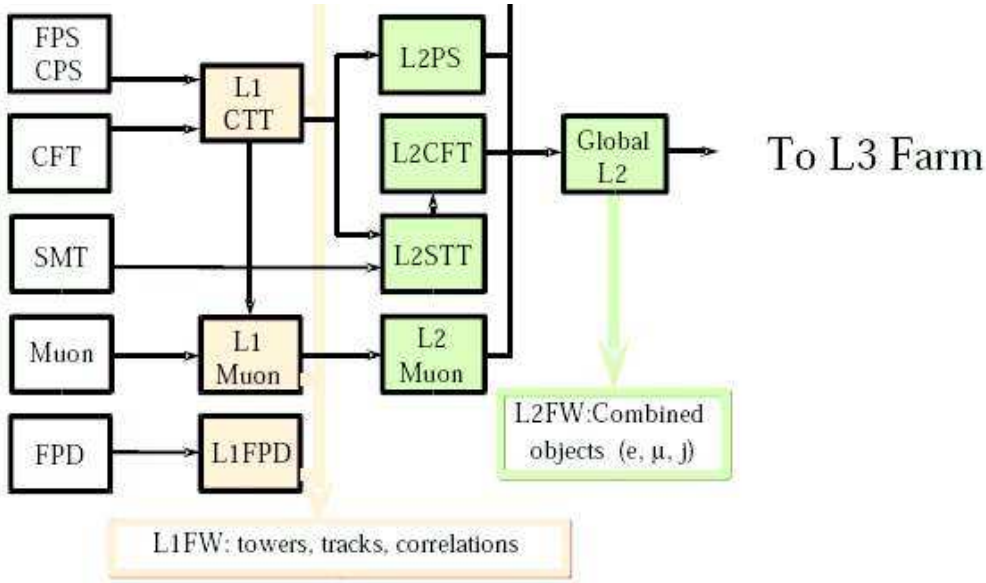

Figure 3.10: The DØ trigger framework

the particles. Three different locations are used to check the availability of the muon track to ascertain the presence of the particle. Out of these three locations, one happens to be outside the toroid, and the other two are inside the toroid. When the presence of a muon is suspected, it is matched with a high pT track which has been ascertained by the tracking detector.

Drift chambers which extend up to η of 2.0 are used for the measurement of hits. The muons leave the gaseous layer or argon mixture ionized. The ionization is transferred onto gold wires held at high voltage. The position measurements are made with the help of checking the time stamp of the arriving ionization pulse. The resolution acheived is around 10 ns. Cosmic ray is shielded during the whole process [18].

3.4.7 Trigger System and Electronics

The protons and anti-protons collide with each other every 360 ns. That makes the frequency of events to be around 2.5 MHz. The limitation of event writing system is capable of operating at 50 Hz due to the long time needed to reconstruct and analyze

the data online. That allows only 1 out of 50,000 bunch crossings to be recorded. The whole mechanism of DØ is based upon three distinct layers of triggers which are needed to filter out only significant physics events.

The detector's front-ends comprise of data coming from sub-detectors like the calorimeter, pre-showers, inner tracker and the muon systems as shown in Figures 3.9 -3.10. Level-1 hardware array accepts electronic signals from the detector front-ends and triggers it down to 5 - 10 kHz depending on the individual need and processing speeds. Level-2 triggering scheme consists of a layer of hardware software combinations dedicated towards bringing down the event rate to 1000 Hz. All the components of Level-2 send data in a common format through Global L2 to Level-3 triggers. Level-3 triggers are a combination of dedicated software which runs on 100 parallel online machines in the control room. This phase reduces the event rate by almost 20 times, writing the final passed events to disk at 50 Hz.

The hierarchy of the trigger mechanism is designed in such a way that an event reaches the next level only after having passed through the previous one. The decision-making at each level is also done by using data from the previous levels [16].

CHAPTER 4

COMPUTING

4.1 Software Framework

The DØ software framework is an object-oriented system which provides the end user common interfaces and methodologies for performing analysis. Generation of application program modules with reception of event data is accomplished through a group of classes. The flow of user-interface points are determined by the framework itself. Usage of functions and pointers are a common protocol defined within the DØ framework and used by all developers of computing and physics concerns.

The main advantage of having a common framework and protocol is the re-usability of code under different circumstances. One can break down a problem into its component parts and shorten effective testing time without getting intimidated by the operating system related details.

4.1.1 Packages

All packages present in the DØ framework are available and maintained through a CVS database repository. The creation of a personal working area with a release version is encouraged before beginning to develop one of your own. Users must derive a new class from a base class named 'package' for their code to become a framework package. It provides a set of utility functions for the framework to interact with the user packages. An example in discussion would be 'l3filters'. This package runs a

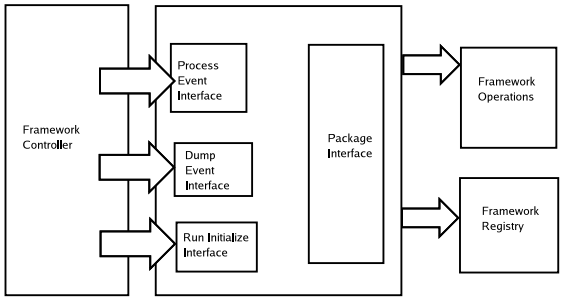

Figure 4.1: Framework

collection of filter codes for the Level-3 triggering system.

4.1.2 Interfaces

The framework is provided with a couple of interface classes (or hooks) which define different points at which a method in the user's package will get called. A user's package implements sets of interfaces with the help of multiple inheritances.

4.1.3 RCP

The Run Control Parameters or the RCPs are library extensions to the framework. These files are used to configure a framework. They are needed in every package instances in order for the package to derive the instantaneous parameters which it would use to produce objects. The parameters could be of any type, provided it runs within the limitation of the system. A typical example of RCP file is filters.rcp, which is used for configuring the package 'l3filters'. The run control parameters are determined by the sequence of tool parameter's minimum, maximum and rms values.

4.1.4 Release and Executables

After compiling the package with the framework, an executable is produced which then can be either run directly through tools or through framework executables. The executables are dynamic links to the compiled code in the local working area. There

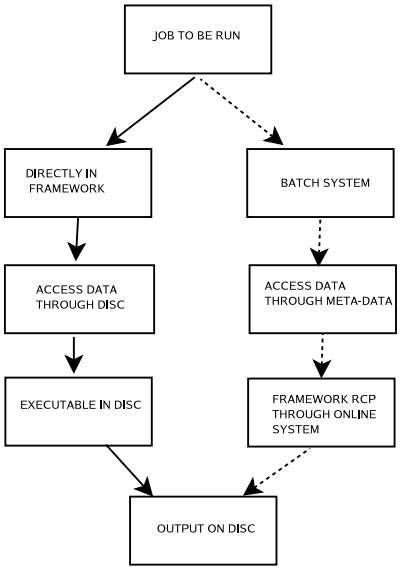

Figure 4.2: A channeled use-case

are 2 different kinds of software releases used in DØ : The test and the production versions. While the test versions are used for packages solely under development stage, the production versions are updated every six months for various releases. The releases are certified and frozen for further usages. The production releases move from software development to online systems and finally towards physics analysis. The versions are named as t/pxx.yy.zz, where the abbreviation t/p represents test or production, while xx represents the major version number. The numbers yy represents changes made within the production version and zz is for additional or special builds made to perform some tests or to satisfy some queries. In a typical release area, the file .baserelease specifies the DØ Run II software version which is currently running. The executables produced after building the area also correspond to the release version. An overlap of 2 different releases in the same working area is not possible.

4.2 Simulation

It is extremely important to cross-check the result of a design over ideal conditions. Simulations of the known interactions determines the dynamics of the particles and

their related geometry. They provide a quantitative background against which resolution and efficiency of the algorithms can be checked.

Monte Carlo simulations are performed over events keeping the same environment as that of a real data event. In the simulated event, knowledge of the physics involved correspond to the expected result. The purity of the selected data sample is checked by performing normalization procedures over real data. Two fundamental steps are used in the generation of Monte Carlo. First, the general physics process is generated. Next, the simulation is fine-tuned according to the specification of the detector [9].

4.2.1 Event Simulation

Computer generated random numbers are used to simulate proton-antiproton collisions. Using the proton density functions, the hard scatter final states are first produced. After this, the showering and hadronization generators are used to produce final state particles. The event generator function has the option of using multiple identity, multiple kinematic information particles. The events are tested over trigger mechanism which have fairly pure acceptance rates. An event generator provides a list of simulated particles simultaneously seen in the detector from an event. A list is produced, which stores the resulting particle's 4-momentum and the vertex information. The hadronic collisions within the framework of the Standard Model tolerance are thus generated. The generation is issued at a center of mass energy $\sqrt{s} = 1.96$ TeV using the Monte Carlo generators [9].

4.2.2 Detector Simulation

The program used to simulate the DØ detector environment is known as the Detector Description and Simulation Tool widely known as GEANT. It is a program which provides the options for passing elementary particles through various materials of different shapes. Before building the actual detector, simulating the experiment

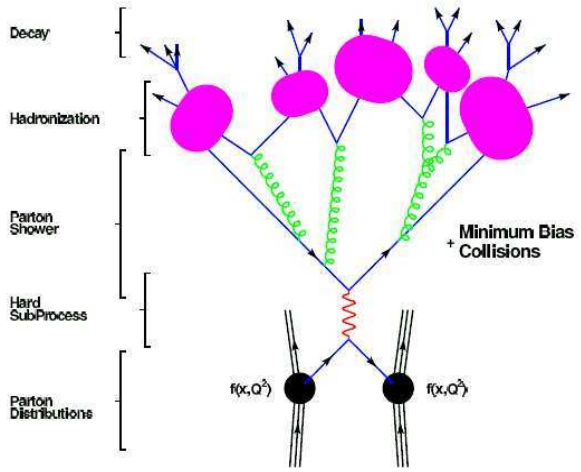

Figure 4.3: Different stages of event simulation

over a software prototype of the same is very useful. This process helps in cutting cost and increasing the lifetime of the components. For DØ the full simulation path consists of DOgstar and DOsim softwares.

The DOGEANT simulation of the Total Apparatus (DOgstar) is a simulation package which generates Monte Carlo studies of the DØ detector at different configurations, for example, magnetic polarity direction of reverse and forward. Simple interfaces of all the sub-detectors are also obtained by the end user. The special run type parameters are then plugged into the simulation like some dead channels or fibers. This process is basically a simulation of background electronic channels.

Although the simulations are done on a full-proof basis, real-time deficiencies of the detector are something which cannot be implemented into the simulation. Additional corrections are applied over simulated and reconstructed events in order to match with the data. For example, some fibers in the CFT become non-responsive to electrical signals because of regular detector wear and tear [9].

4.3 Storage and Network

The huge volume of data of various formats which form the output of triggers, simulations, and analusis results need to be stored and archieved. SAM or Sequential Access to Meta Data is a data analysis and handling system managed through an array of servers running CORBA. The utility of SAM helps to access, store, and retrieve data files of various types and utilities [15].

Datasets, Snapshots, Consumers, Projects, and Stations are concepts around which SAM runs. The consumer is a user application who requests the running of projects on a particular station. An additional request is placed with the station regarding the delivery of the output files to one or more consumers on the station. The station, which is a collection of hardware resources, runs executables against snapshots or datasets. The datasets on the other hand had been definitions created by the user before. They are customized with various parameters to meet the exact need of the consumer. The delivery of files to the station cache are temporarily protected from deletion until the consumer issues a signal for the same.

A common minimum protocol is followed by the administrators and the station masters. Communication is handled through a middle layer process called with a data base server. The server runs a python script in order to communicate between the database and other SAM components using CORBA. SAM file storage servers are employed by the various DO offline Monte Carlo production centers and DO online systems. A desktop cluster linux system (CluedO), a linear System reconstruction Farm (CAB), and the primary unix machine D0mino(1-4) form part of the SAM onsite system for the DØ collaboration. Remote SAM stations are united in a grid formation with a batch submission system using CONDOR and GLOBUS grid tools.

CHAPTER 5

DESIGN AND ALGORITHM

The design parameters for the final event selection is subjected through numerous variables and run control parameters. Since the framework has an object oriented approach, interfaces with various tools at different phases of the algorithm are implemented. The muons, jets and tracks run through their individual array of programs which are called sub-algorithms. Successful candidates are recorded at every stage. All the tools used and implemented are part and parcel of the Level-3 framework.

Level-3 framework is a special subset of the central CVS repository. This framework consists of individual tools (within independent packages). Individual physics groups are responsible for maintaining and running objects. For example, Level-3 possesses in its armory, jet, b-tagging, muons, and tracking etc. Differnt id groups are responsible for handling the proper physics events being written to disk after being accepted by the trigger framework successfully. Since the time taken for each tool to fire for every event is an important issue due to the limitation of speed of writing on disk, it is extremely important that algorithms developed for each group is fast enough to suit its need. At the same time, optimization is needed to speed up the process of saving key phyisics events.

Triggering at Level-3 is done through a reference file named level3.sim file. This file is a master copy of the triggering schemes used for every test or production version of the software packages. Each .sim file produced also corresponds to the software

version release used to configure it. In the design of the muon-tag filter, the first release version where it was added to the repository was p17.04.00. The .sim file has been a development over version 13.51, which was running on the online L3 farm machines using p16.04.00.

A general flow of logic of the new code has been explained with the help of a flowchart in Figure 5.1. In the first phase of the algorithm, jets, muons, and track candidates are selected. In the second phase, the candidates are run through dR matching algorithm for checking the presence of valid candidates.

5.1 Jet Algorithm

Jets are particle showers which originate due to hadronization and leptonic decays in the calorimeter of the DØ detector. The origin of jets are due to quark-antiquark meson pairs. A typical jet formation in the DØ detector is shown in Figures 5.2 and 5.3 in transverse and longitudinal sides, respectively. Calorimeter jets are characterized by towers or sectors in the η-ϕ plane. The third dimension is the energy distribution in each tower.

5.1.1 Jet Parameters

Though the obvious choice for jet geometry would be θ , ϕ and z , θ is not suitable for Lorentz invariance. The reason is because the differential increment in the value of the angle in the longitudinal section of the detector is incapable of providing uniformity of reaction when Lorentz corrections are made. Hence, the pseudorapidity η suits the role perfectly. The mapping of η with θ is as follows:-

$$\eta = \ln(\tan(\frac{\theta}{2}))$$

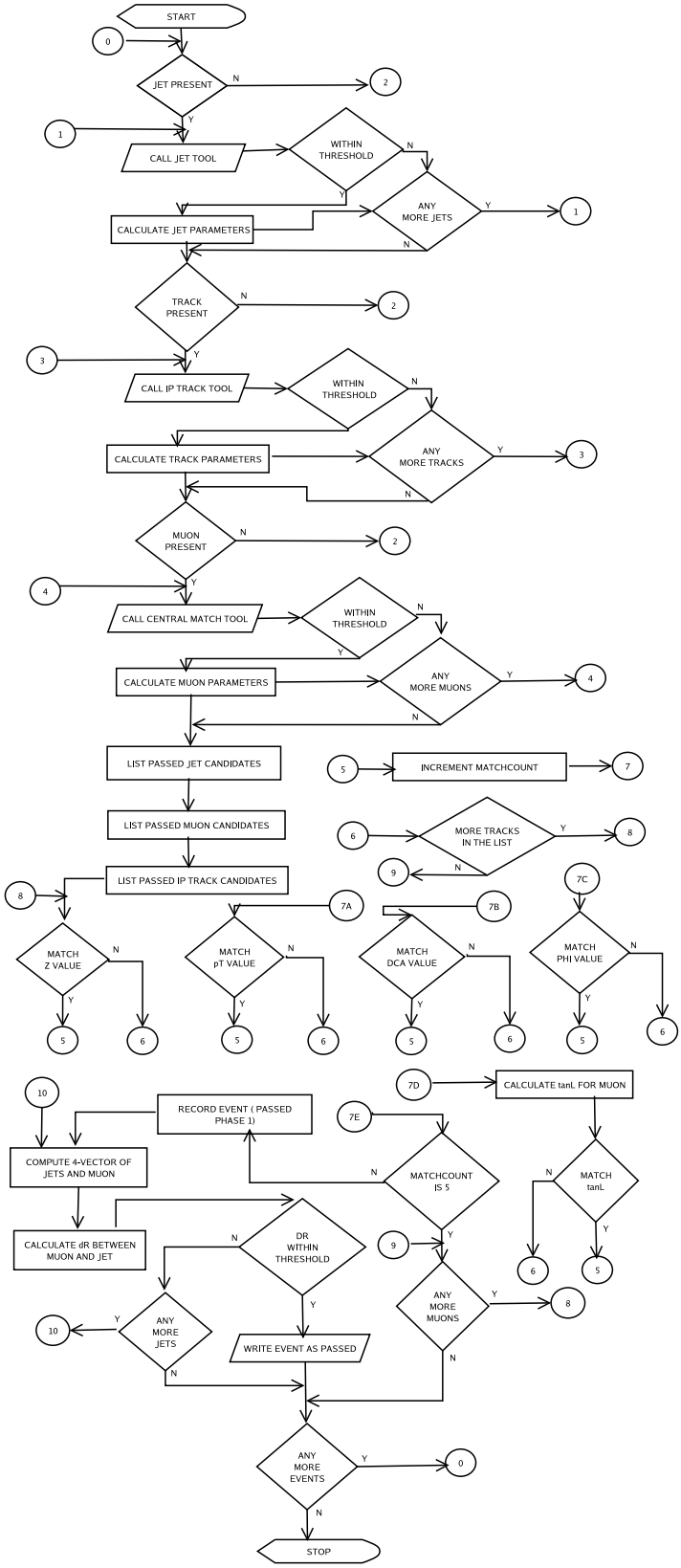

Figure 5.1: An overview of the algorithm with flowchart

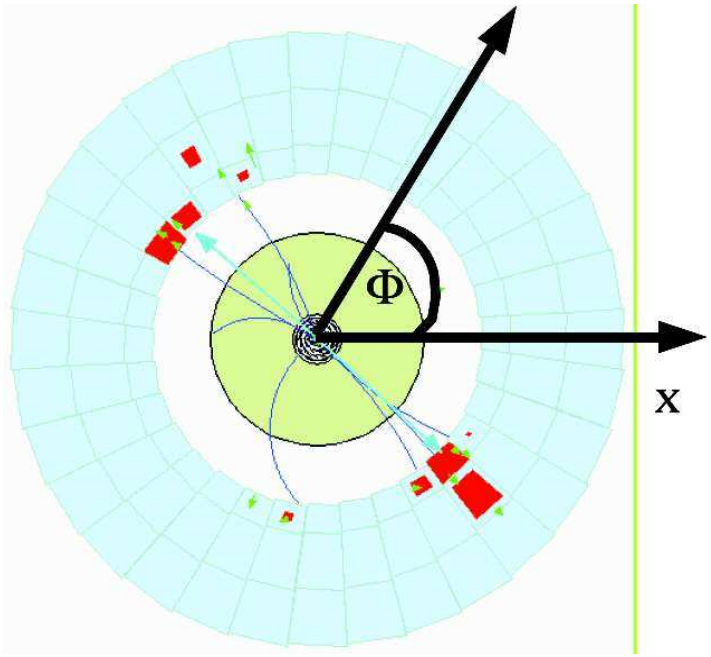

Figure 5.2: Transverse view of the jet with ϕ

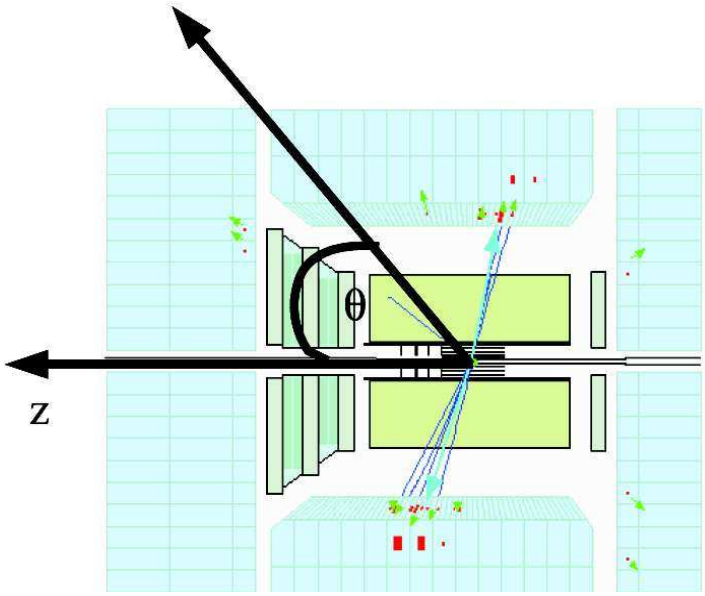

Figure 5.3: Longitudinal view of the jet with Z and θ

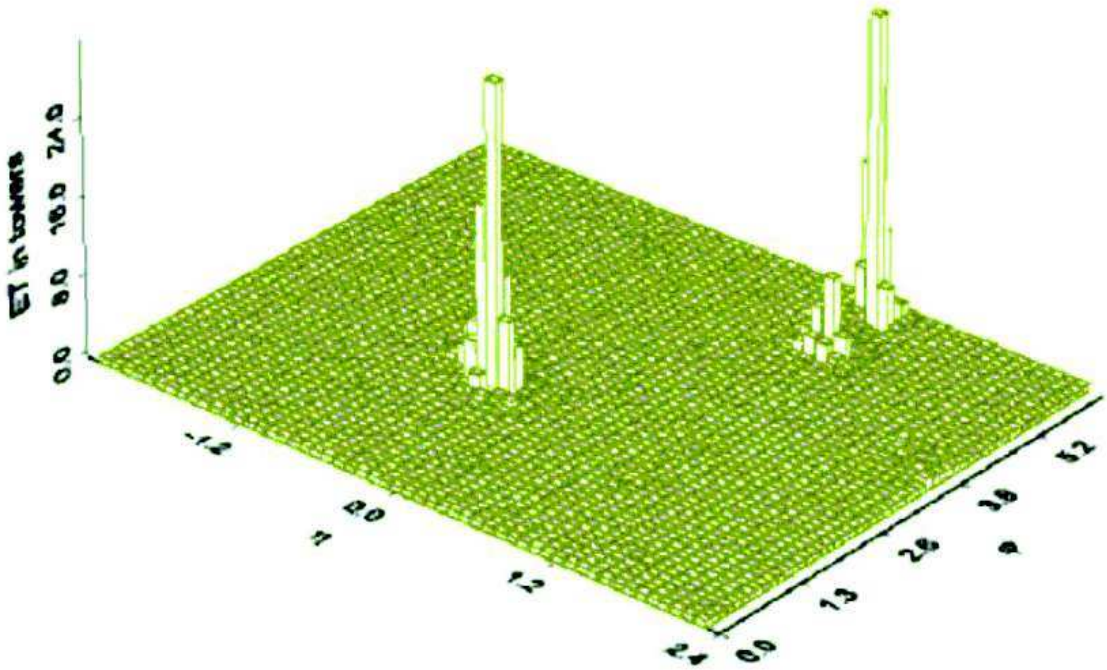

Figure 5.4: A projected 2-3 jets in the η - ϕ plane

Within high energy approximation, the value of η only changes by an additive constant. During the jet classification process, the weightage of high energy particles within a jet should be kept more than the ones with comparably lower energies. The direction resolution is perfected by the above mentioned parameters. The transverse energy E_T is weighed against all the individual contributing energy deposits within a cluster. E_T is given by

$$E_T = E \sin\theta$$

E_T, being Lorentz-invariant, also serves the purpose served by η. Hence, the three parameters finalized upon are ϕ, η, and E_T. Mapping the jet on a three-dimensional lego plot is a common practice within experiments. Figure 5.4 provides a generic example of one such plot.

5.1.2 Locating Centers

A seed is defined as a tower with E_T greater than E_0 (the average energy deposit in a cluster). First, the exact cell is located from a list of cells present in the η - ϕ plane. The geometric center of the circle with radius R is assigned to the seed cell. A summation of all the other energy deposits are taken for cells within a threshold of R. The energy-weighted centroid is calculated in order to find out the area of focus within the circle with radius R. If the new centroid is found to be the same as that of the geometric center, then the cluster is passed. If it fails the test, then the next geometric center is the newfound energy-weighted centroid of the cluster. This way an iterative process is used until the geometric center and the energy-weighted centroid match exactly.

The list of clusters with their respective centers are then passed on to the split/merge algorithm to resolve the conditions of jet overlaps. Figures 5.4 and 5.5 explain the process of finding centers. This is an approximation series likethe gauss-siedel method. The formulas used for iterations are provided below where C denotes centroid and i denotes the seed.

$$R = \sqrt{(\eta^i - \eta^C)^2 + (\phi^i - \phi^C)^2}$$

$$\eta^C = \frac{\Sigma E_T^i \eta^i}{E_T^C}$$

$$\phi^C = \frac{\Sigma E_T^i \phi^i}{E_T^C}$$

$$E_T^C = \Sigma E_T^i$$

5.1.3 Jet Overlap

There is a possibility that two adjacent jets could overlap. In that case η - ϕ cells located are traced and run through a split/merge algorithm. The highest towers

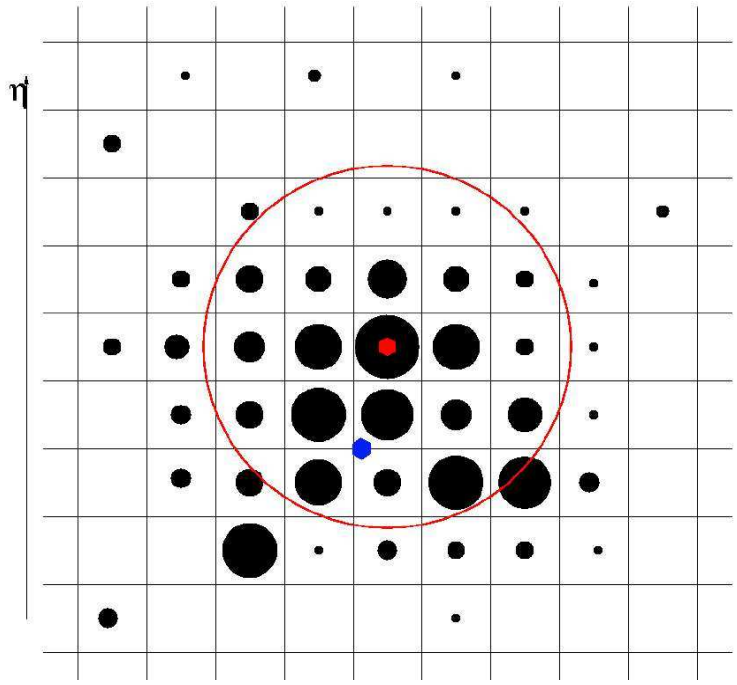

Figure 5.5: Center and centroid do not match

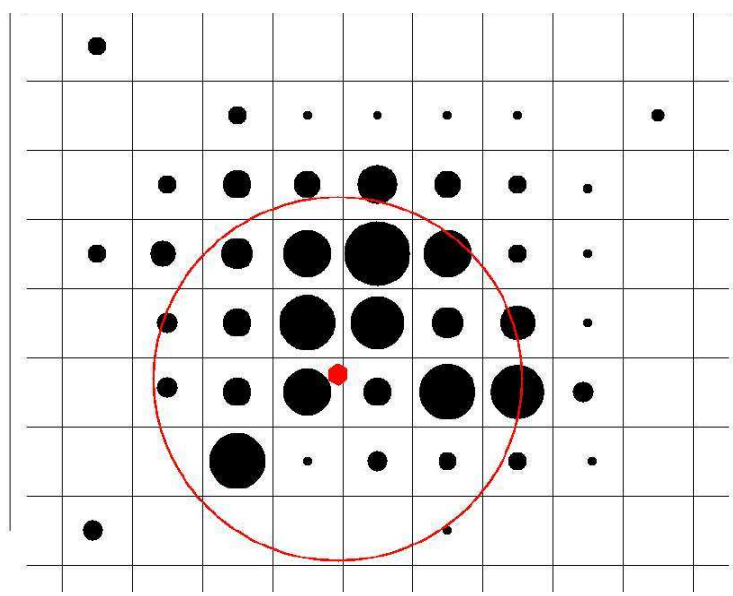

Figure 5.6: Centroid and geometric center matches

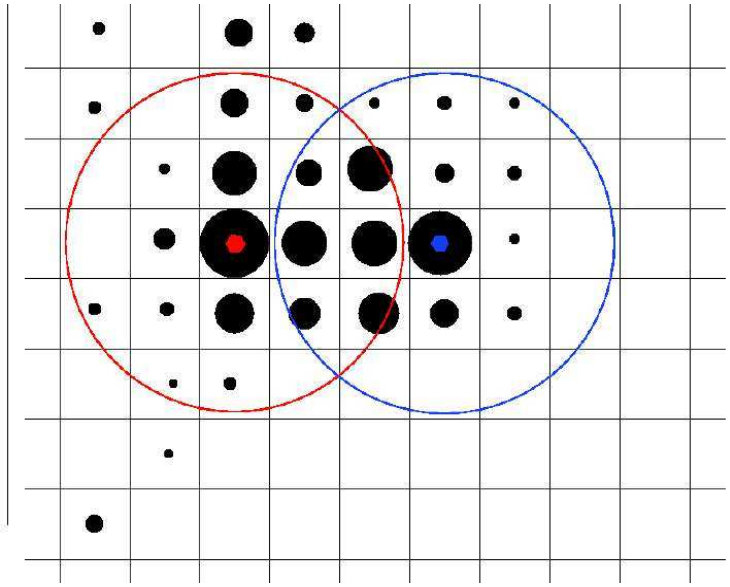

Figure 5.7: Split jets with two different towers

after finding the centroids are matched with each other. If the ratio of the energy deposition is greater than a calculated threshold with reference to one of the jets, then the neighbouring jet is merged into the reference jet. If the ratio is below threshold, then both the jets are split and the common cells (shared) are assigned to the jet with the nearest centroid in the η - ϕ plane. Figure 5.7 displays 2 split jets with shared cells [14].

5.2 Muon Algorithm

The muon detector detects muons using three different segments as already described in Chapter 3. There are two different kinds of muon tracks found solely through the muon detector. The first category is called the A-stubs and they are tracks found without any segment hit on B and C layers. The other type of tracks or the global muon tracks are the ones found through hits in all three A-, B-, and C-layers. The A-layer hit is a prerequisite for a track to be termed as a muon track. The tracks are characterized by a position on the track before and after the toroid. The positions

have a 1 mm resolution in the drift-plane. The 3-momentum of the vector is found in these regions [18][3].

Due to low occupancy rates in the muon detectors, the track reconstruction in the muon systems is relatively faster than the ones in the other regions of the detector. The pT resolution of muon tracks is quite low. Hence, the muons need to be matched with a central track in order to improve the pT resolution of the overall system. Matching muons to central tracks involves predicting the region for hits in the inner tracker. It also involves using the Global Tracker Algorithm. This algorithm is chosen since it uses both CFT as well as SMT hits.

5.2.1 Extrapolation

Since the hit occupancy in the CFT is higher than those in the muon system, it takes more time to reconstruct the tracks. So, a small section of the CFT is sectioned out for evaluation. It is required that the tracks should project out of the CFT through a curved rectangle with ϕ and Z ranges. The radius R is kept fixed at 51 cm. The central tracks also need to have polar angles at this range. The lower bound on Z is found by considering the lower bound of Z in the curved square and the highest allowed polar angle. The higher bound on the Z vertex of the region is found by using the lower bound on the polar angle.

In the muon system, every track has attributes of ϕ and θ of the tracks with errors. Multiple scattering in the calorimeter is calculated at $\frac{200}{pT} + 3$ cm (emperical). The prediction of the region is done by using the extrapolated track through the calorimeter and using a value of 3σ on reconstruction. For the hard scattering, a value of 4σ is used.

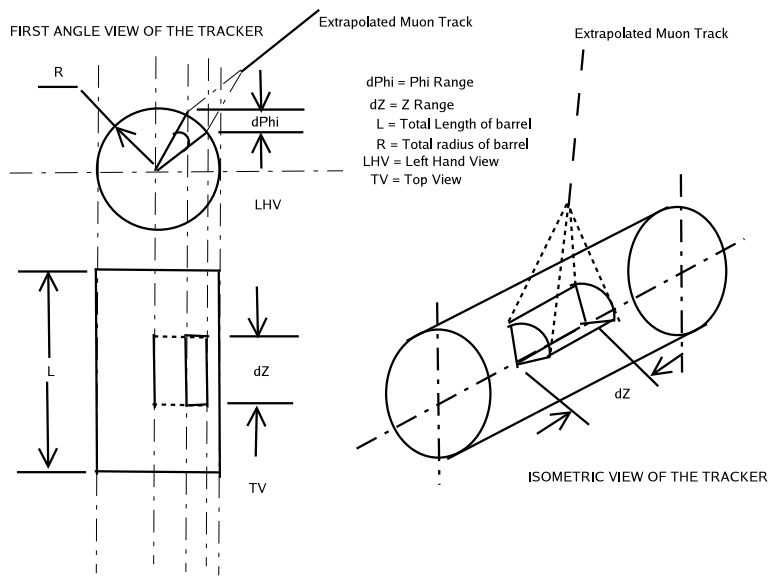

Figure 5.8: Central match with CFT

5.2.2 Central Match

All tracks need not match the muon tracks. Hence, the program loops over the list of tracks to find a good χ^2 fit between the tracks. The tracks from the CFT are extrapolated to the A layer of the muon region with a straight line. Although the calorimeter impose a 2.0T return field on the tracks, because of the solenoid, multiple scattering makes the bend negligible.

The extrapolated tracks are matched with the θ and ϕ values of those of the muon tracks. The third parameter used is called the δ drift. It is the direct displacement between the extrapolated tracks and the muon tracks. In the central region of the muon detector, the distance is measured in the z-axis. In the forward region, the distance is measured in either x- or y- direction depending on the octant used. The fit parameters are shown below [2].

$$\chi^2 = \frac{1}{3}((\frac{\delta(drift)}{\sigma_\delta(drift)})^2 + (\frac{\delta(\phi)}{\sigma_\delta(\phi)})^2 + (\frac{\delta(\theta)}{\sigma_\delta(\theta)})^2)$$

5.3 Track Fit

As shown earlier in the flowchart diagram, the track-fit between the muons and tracks make use of 5 different parameters. The quality of muons selected are all of central matched type. Hence, for any muon track present in the second phase of the filter, a considerably well defined track is present in the central region of the detector. Since the search is for b-quarks, the preliminary criteria is to have a high impact parameter supplementing the quality of tracks.

Impact Parameter tracks are a subset of global tracks which are found using axial and stereo tracking algorithms. They have a vicinity with the primary vertex (the initial interaction point). Figure 5.9 explains the five parameters used to match the central-track muons and the IP tracks. All track parameters in Level-3 are represented in the form of a five-helix structure.

The definition of the parameters is as follows:

1. $P_T^{-1} = \frac{B_o qc}{R}$: This means the inverse track momentum. B_o is the strength of the magnetic field and q is the charge of the particle. The radius R is the radius of curvature in the x-y plane. If q is positive, then the track turns anti-clockwise in reference to the x-y plane and vice versa.

2. ϕ_0 : This is the azimuthal angle of the track momentum at the point of closest approach to the z-axis.

3. $tan\lambda = \frac{dZ}{dS_xy}$ is the pitch. It is basically the ratio of the distance traversed in Z direction to the distance traveled in an arc in x-y plane.

4. DCA = S x d_0 : It is called the Distance of Closest Approach. d_0 is the positive

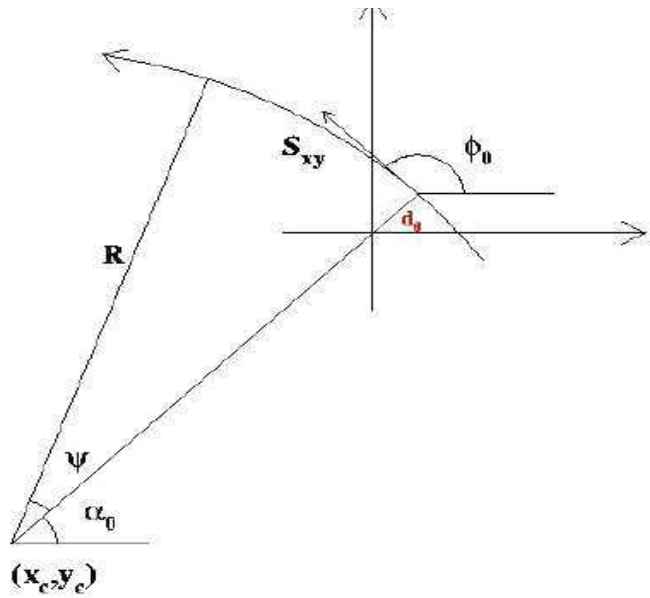

Figure 5.9: Track Parameters in X-Y Plane

distance between the origin and the point of closest approach to the z-axis. S indicates the sign of the angular momentum of the track about the origin.

5. Z_0 : This is the position of the track on the z-axis at Distance of Closest Approach [1].

One more advantage of using the IP tracks is that the impact parameter value can be used in providing additional thresholds to the filter.

5.4 dR Calculation

The final part of the algorithm involves calculation of dR or the incremental radius cone of the jet with respect to the muon. Each cone corresponds to towers in the calorimeter. A typical dR for jets is calculated by dR= $\sqrt{\delta\eta^2 + \delta\phi^2}$. In this case the differential η and ϕ values are calculated as follows :

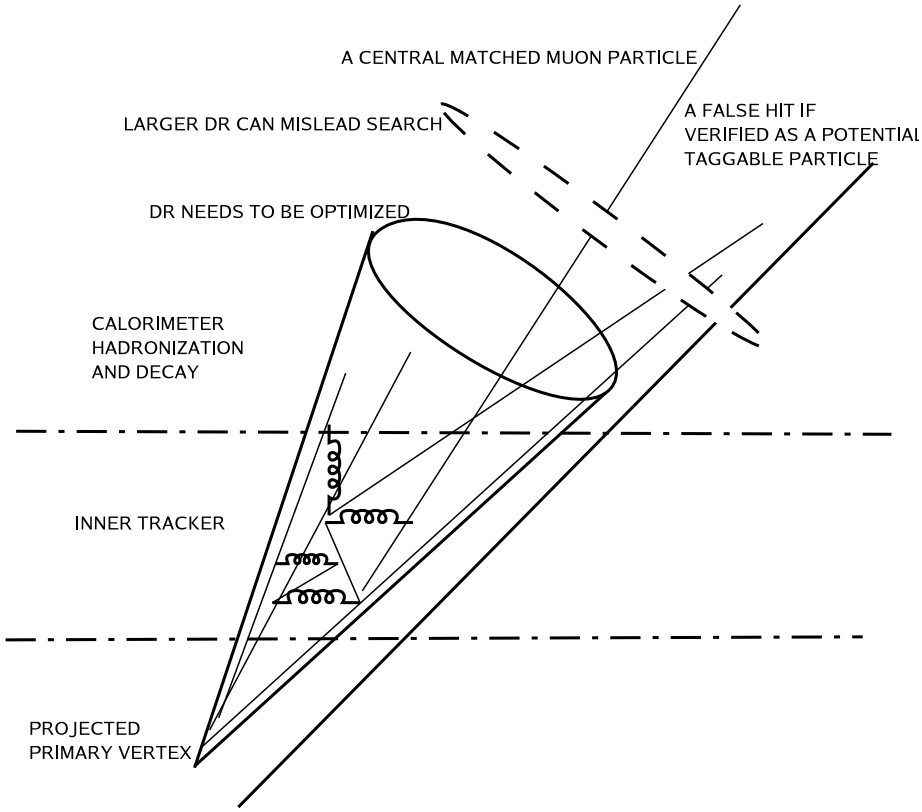

Figure 5.10: Primary vertex location and jet reconstruction

1. $\delta\eta = abs(MUON_\eta - JET_\eta)$

2. $\delta\phi = abs(MUON_\phi - JET_\phi)$

The cone-size increment of the value is important since any stray muons not involved with the jet could be trapped within the dR.

CHAPTER 6

RESULTS AND CONCLUSIONS

The procedure for testing and certifying a code within the DØ framework is rigorous. The process involves testing the method against substantial Monte Carlo and real Run II data events. In order to gain efficiency in the control room while data-taking, rejection in the real-data is important. At the same time, the rejection should not be at the cost of significant loss of physics information.

6.1 Preliminary Comparisons

Different samples of $Z \rightarrow$bb MC files have been used in order to certify the preliminary findings. The sequence of filters in the framework trigger being L3FJets, L3FIP, L3FMuon, L3FBTagMU,and L3FMarkAndPass. The main comparisons are performed with the help of Z→bb MC events and monitor stream Run II data from an old run. In the present case, run number 202097 has been used to see the effect of the algorithm on real data. Following are the steps used for the tests:

- Compilation of the code into an executable with the package for trigger simulation.
- Change in configuration in the run directory for offline running with a speciliazed triggerlist.
- Running the root interpreter with the analysis package to obtain desired results

Table 6.1: Events passed by the filter hierarchy within the trigger

Data and MC Events		
Filter	Events Passed(Data)	Events passed(MC)
Initial	3000	3000
L3FJet	1335	2839
L3FIP	1180	2178
L3FMuon	137	333
L3FBTagMU	34	144
L3FMarkandPass	34	144

[21].

In both cases of MC and data, 3000 events were considered in the beginning. They were passed through a series of filters within a trigger. Table 6.1 provides the breakup of events for both the MC and data.

6.2 Jets

The jet detector distributions for both the Z→bb MC and data show similar trend in distributions for all unbiased events. As shown in the table in the previous section, the rejection of events in the three preliminary stages on the algorithm is higher in the case of data as compared to that of the MC. Due to this, the total output of events gathered through MC is higher by roughly 20% than that of the data. Since this could be misleading, an independent efficiency study has been performed, explained later in the chapter.

A standard gaussian function F(x) = $\frac{1}{\sigma\sqrt{2\pi}}e^{\frac{-(x-\mu)^2}{2\sigma^2}}$ has been used to fit all the plots.

6.2.1 η Distribution with All Events

The initial distribution for the Jet η provides a mean of μ=0.02744 with σ=1.38 for Z→bb MC. On the other hand for the data μ=-.01842 with σ=1.4965. The unusual peak or surge at η=1.0 in data is because of the misfiring inner cryostat detector

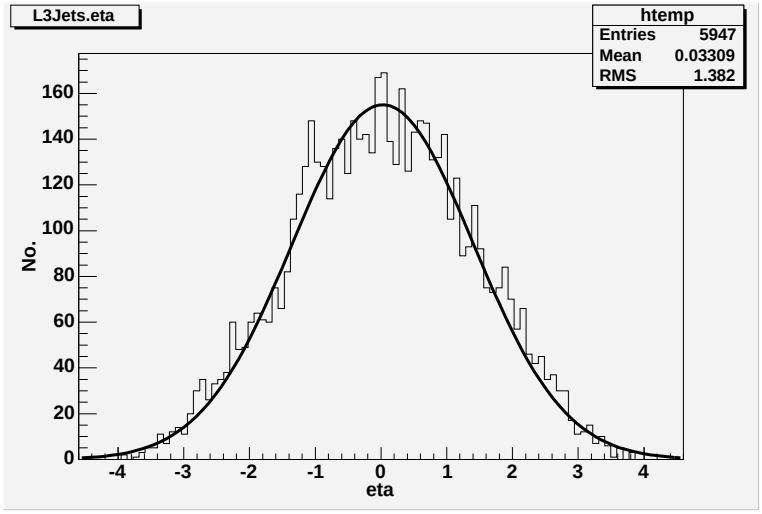

Figure 6.1: Jet η distribution with all events in MC

(ICD). The difference in mean $\delta\mu$ between data and MC is 0.04586.

6.2.2 η Distribution with Rejected Events

The selection of events were performed by keeping the L3Unbiased trigger bit equal to 0. Since the L3MarkandPass filter forms the last filter in the sequence within the trigger, all events passed by it are basically the events passed by the trigger as a whole. If the trigger bit returns a 0, then the trigger fails for that event. The failure is attributed to the filter rejecting the criterias in the algorithm. The rejection of events in MC for the Jets η project a mean of 0.015644 with σ=1.436. The shift in mean due to rejection of events in MC is $\Delta\mu = 0.011796$. The rejection of events in data for the Jets η project a mean of -0.03808 with σ 1.5044. The shift in the mean due to rejection between the monitor stream data is $\Delta\mu$=0.01966.

6.2.3 η Distribution with Accepted Events

The selection of events were done by simulating the condition for L3Unbiased trigger bit equal to 1. The acceptance in MC or the Jets η project a mean of 0.08643 with σ=1.97. The shift in mean due to acceptance in MC is $\Delta\mu$=0.05899. The acceptance

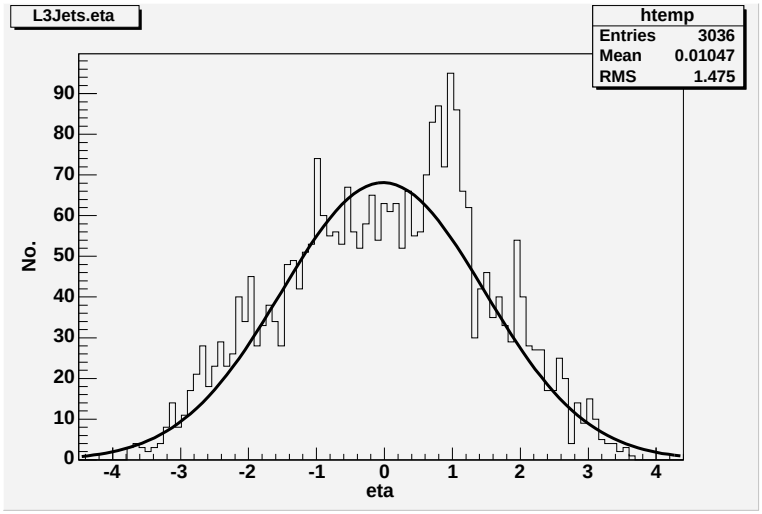

Figure 6.2: Jet η distribution with all events in data

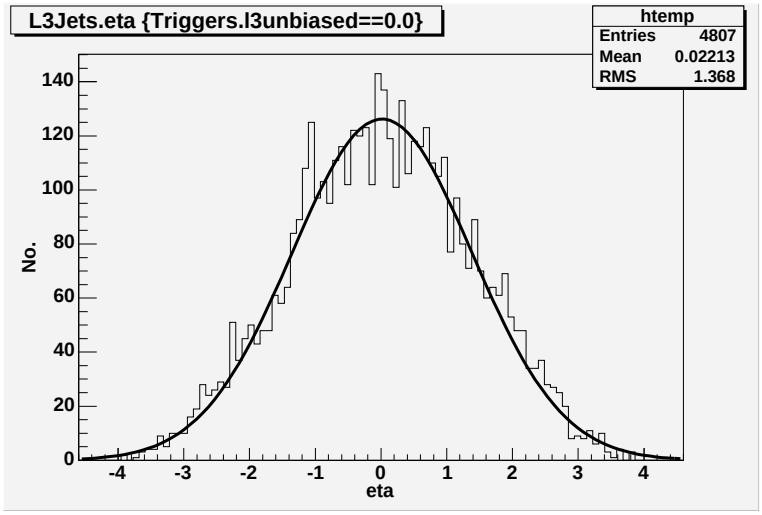

Figure 6.3: Jet η distribution with rejected events in MC

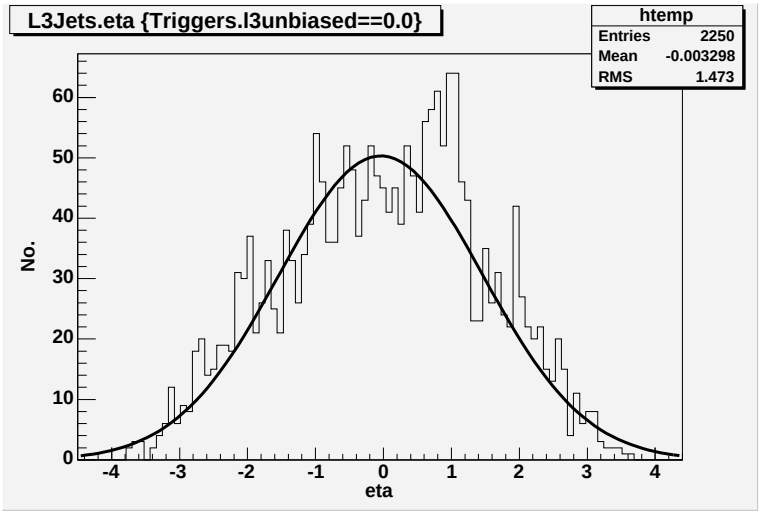

Figure 6.4: Jet η distribution with rejected events in data

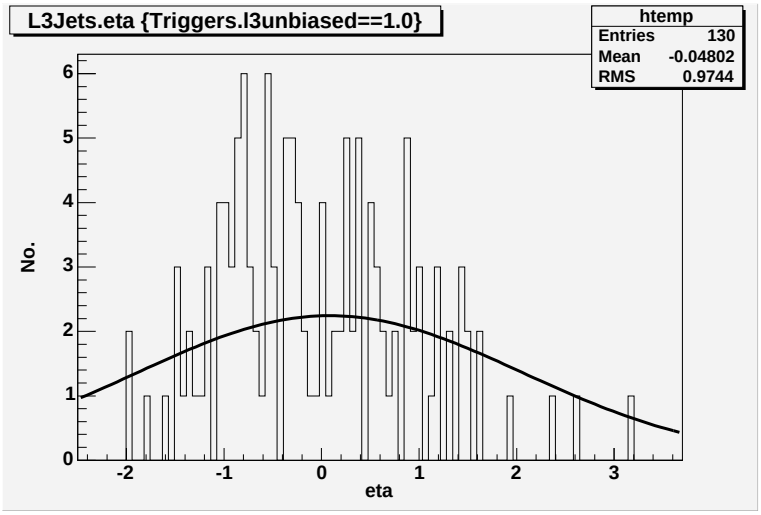

Figure 6.5: Jet η distribution with accepted events in MC

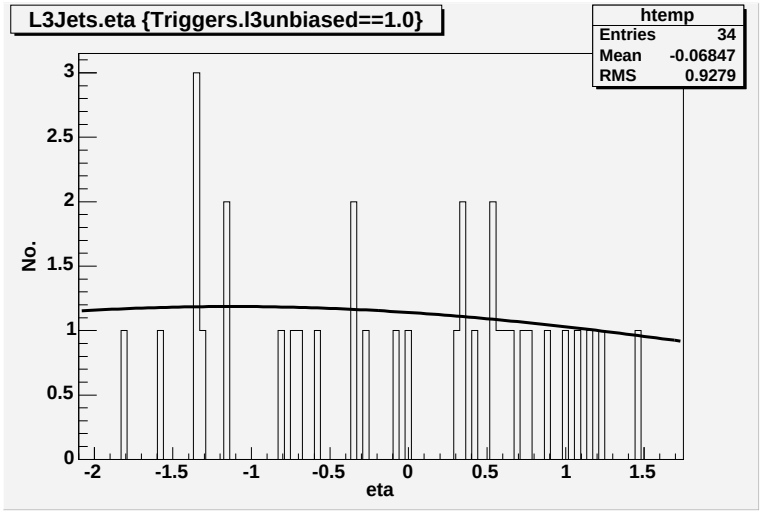

Figure 6.6: Jet η distribution with accepted events in data

of events in data for the Jets η project a mean of -1.124 with σ=3.985. The shift in mean due to acceptance in the monitor stream data is $\Delta\mu$=1.4242.

6.3 Muons

Since the η of the muon and the η of the jet etas need to be matched for calculation of dR; hence, checking the distribution of muons with respect to the detector becomes extremely important.

6.3.1 η Distribution with All Events

The initial distribution for the Muon η provides a mean of μ=0.04157 with σ=0.935 for Z→bb MC. On the other hand for the data μ=0.02808 and σ=1.24. The difference in mean $\delta\mu$ between data and MC is equal to 0.06965.

6.3.2 η Distribution with Rejected Events

The rejection of events in MC for the Muon η project a mean of 0.071328 with σ=0.9679. The shift in the mean due to rejection in MC alone is $\Delta\mu$=0.029158. The

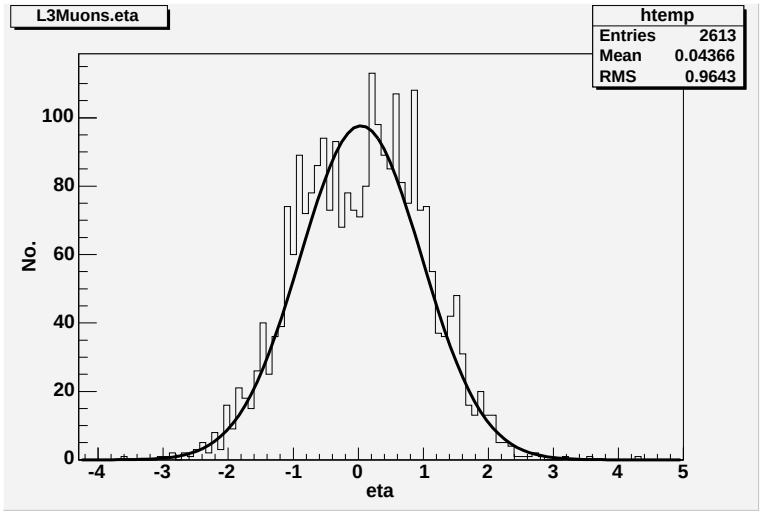

Figure 6.7: Muon η distribution with all events in MC

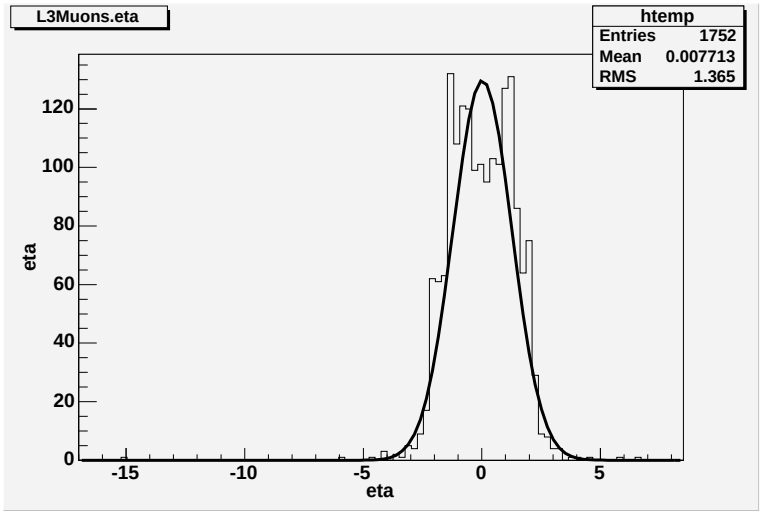

Figure 6.8: Muon η distribution with all events in monitor stream

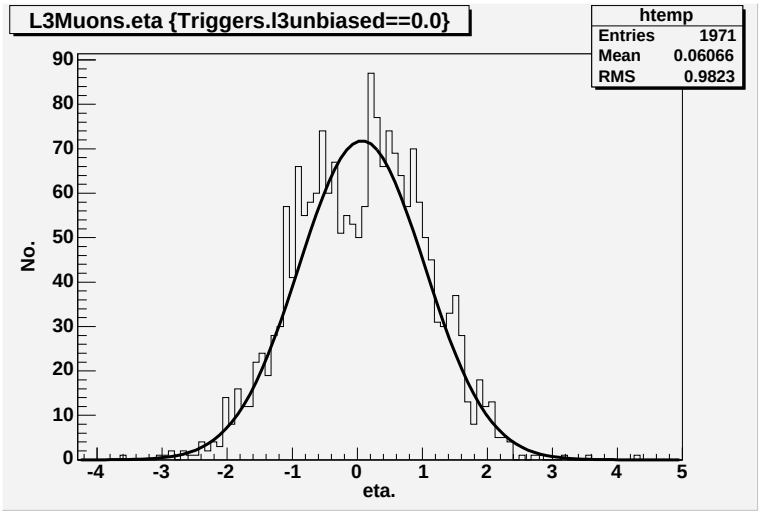

Figure 6.9: Muon η distribution with rejected events in MC

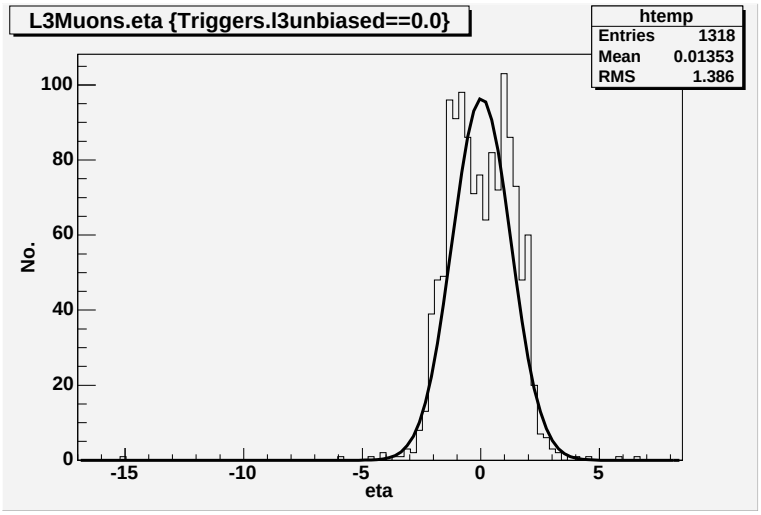

Figure 6.10: Muon η distribution with rejected events in data

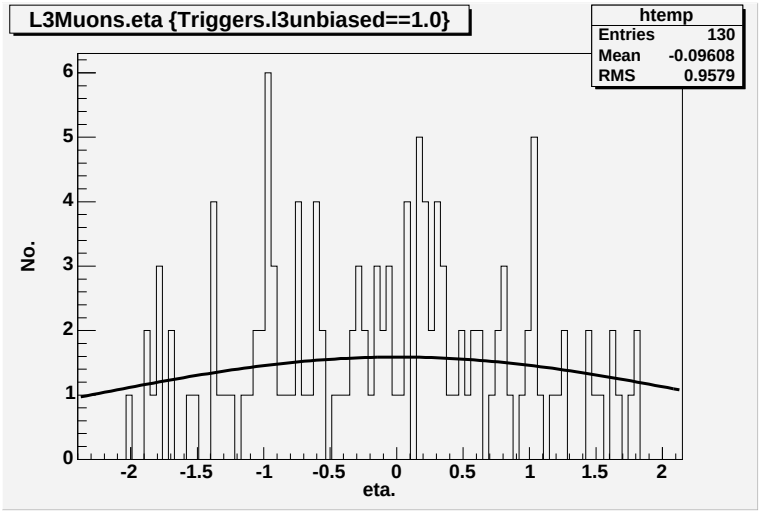

Figure 6.11: Muon η distribution with accepted events in MC

rejection of events in data for the Muon η project a mean of 0.03164 with σ=1.24. The shift in the mean due to rejection of events in data alone is $\Delta\mu$=0.00356.

6.3.3 η Distribution with Accepted Events

The acceptance of events in MC for the Muon η project a mean of 0.01002 with σ=2.4. The shift in the mean due to acceptance in MC events alone is $\Delta\mu$=0.03155. The acceptance of events in Data for the Muon η project a mean of 0.01 with σ=2.5. The shift in the mean due to acceptance in the monitor stream data is $\Delta\mu$=0.01808.

6.4 Impact Parameter Tracks

Although 5 different parameters are used to match with the muons, the Z0 is by far the most significant parameter [22]. Z0 forms a vicinity cut with the primary vertex of the jet. A good fit with Z0 ensures better resolution in Phase I of the filter design.

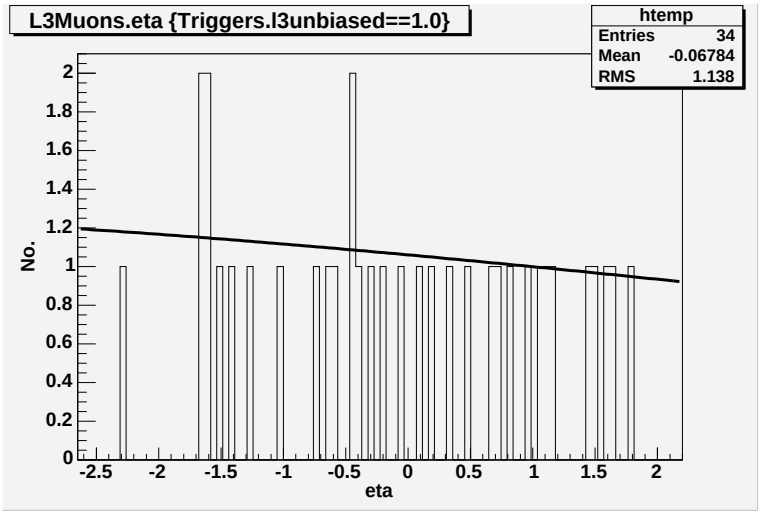

Figure 6.12: Muon η distribution with accepted events in monitor stream

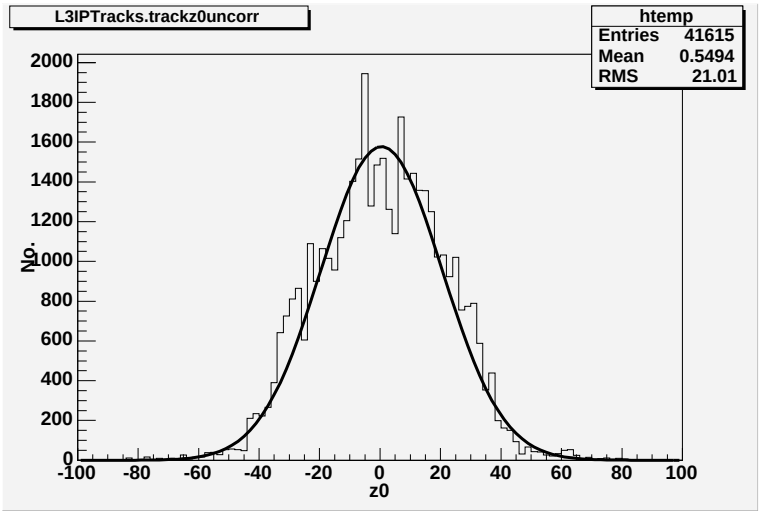

Figure 6.13: Z0 distribution with all tracks in MC

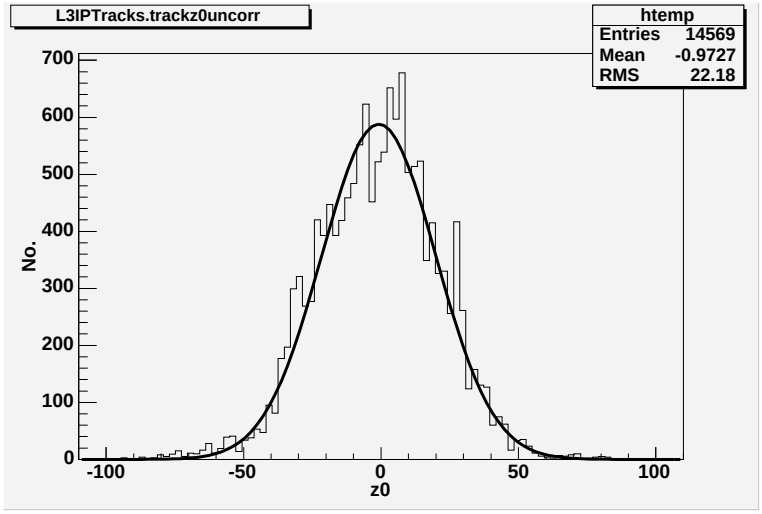

Figure 6.14: Z0 distribution with all tracks in monitor stream

6.4.1 Z0 with All Events

The initial distribution for the IP Z0 provides a mean of μ=0.515 with σ=20.06 for Z→bb MC. On the other hand for the data the μ=-0.8178 with σ=20.80. The difference in mean $\delta\mu$ between data and MC is equal to 1.3328.

6.4.2 Z0 with Rejected Events

The rejection of events in MC for the IP Z0 project a mean of 0.0343 with σ=23.27. The shift in the mean due to rejection in the MC alone is $\Delta\mu$=0.172. The rejection of events in data for the IP Z0 project a mean of -0.6199 with σ=24.13. The shift in the mean due to rejection in data alone is $\Delta\mu$=0.1979.

6.4.3 Z0 with Accepted Events

The acceptance of MC events for the IP Z0 project a mean of 1.789 with σ=35.59. The shift in the mean due to acceptance in the MC alone is $\Delta\mu$=1.274. The acceptance of events in data for the IP Z0 project a mean of -0.1230 with σ=57.9. The shift in mean due to acceptance in the monitor stream data alone is $\Delta\mu$=0.6948.

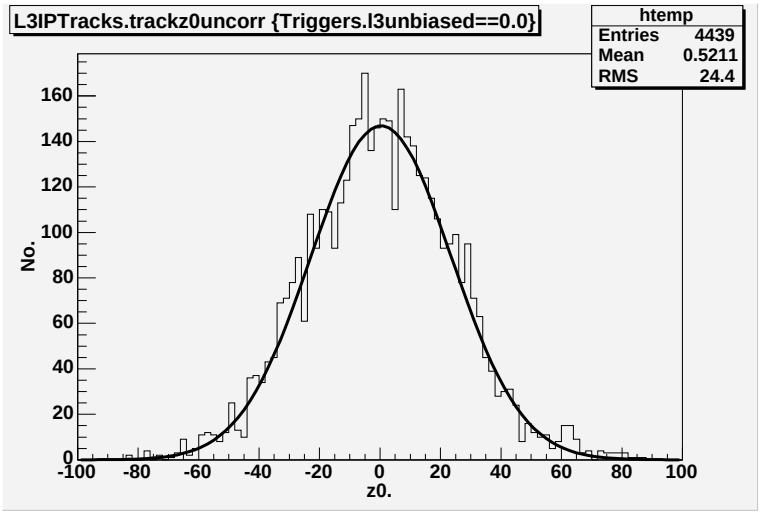

Figure 6.15: Z0 with rejected tracks in Z→bb MC

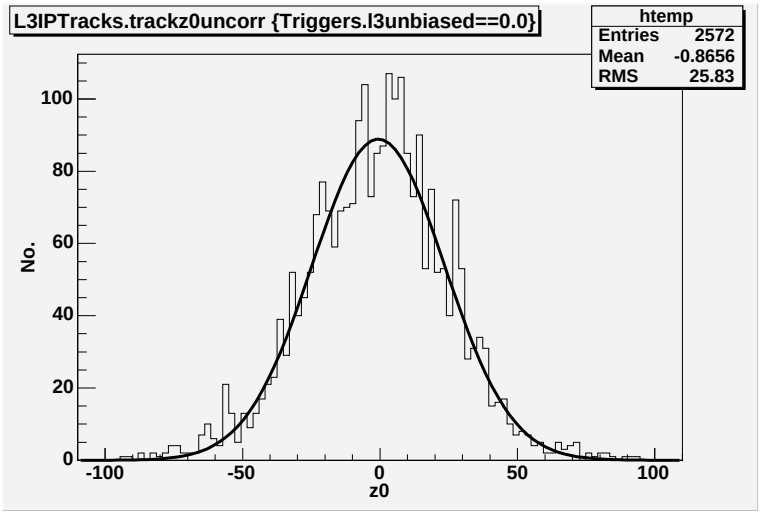

Figure 6.16: Z0 with rejected tracks in monitor stream

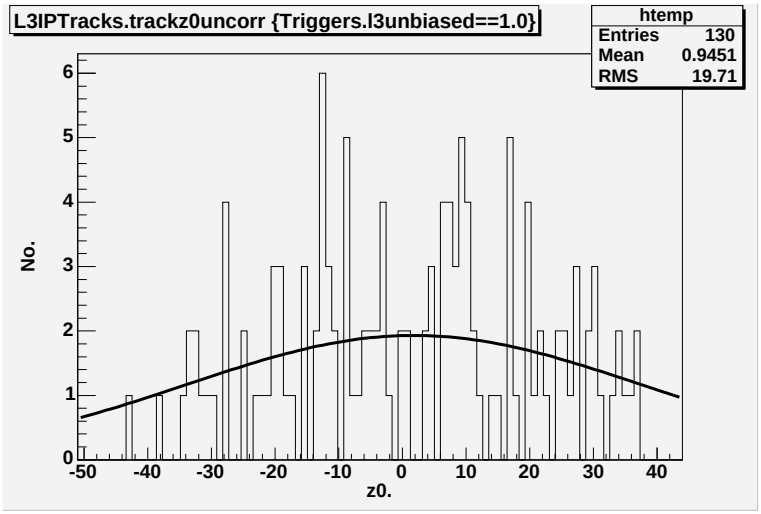

Figure 6.17: Z0 with accepted tracks in Z→bb MC

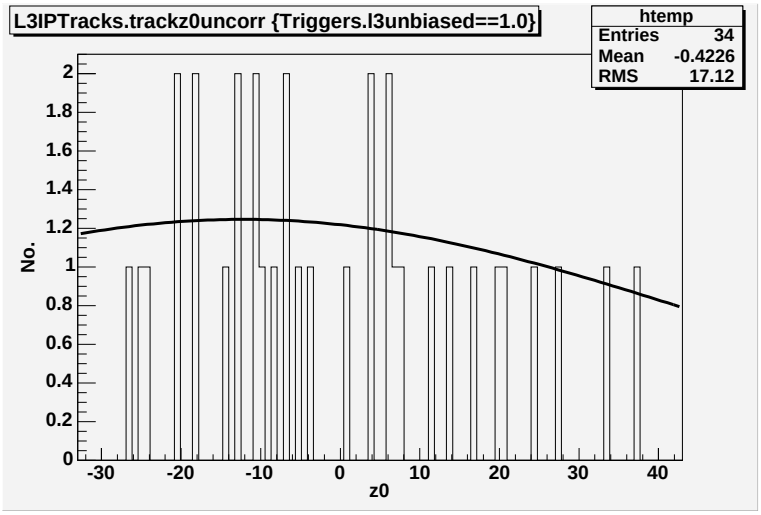

Figure 6.18: Z0 with accepted tracks in monitor stream

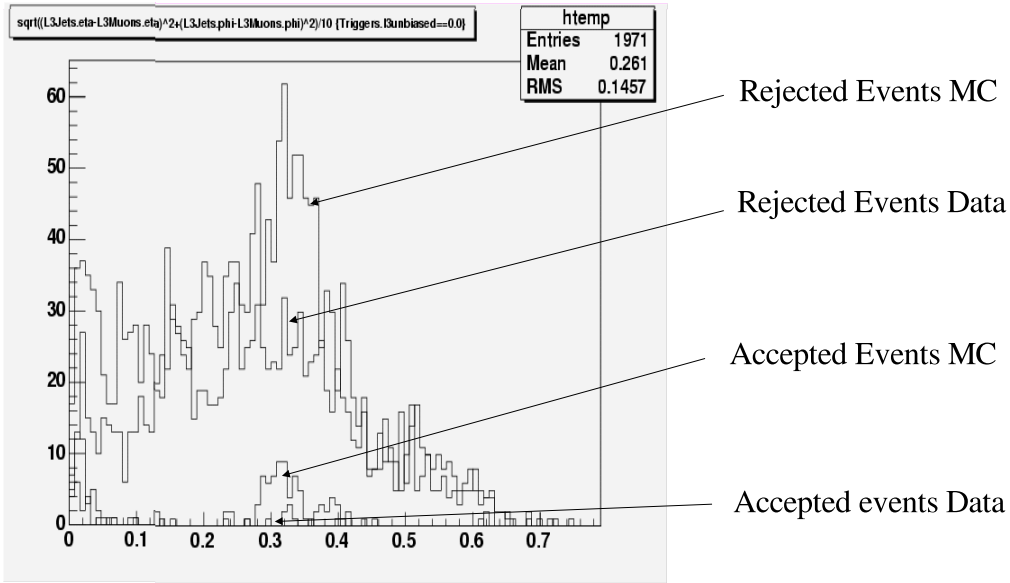

Figure 6.19: The distribution of all events against a simulated dR for acceptance and rejection

6.5 Rejection Distribution and Stringency Check

The total distribution of the events against a simulated dR is a good visual check of the overall performance of the algorithm. Figure 6.19 provides such a view. Rejection and acceptance have been plotted on a common canvas. In order to cross-check the rightfulness of the study, a cumulative table with the number of jets left over as opposed to the absolute value of the difference between the η values of the corresponding jets and muons have been produced. When plotted against each other it was noticed that even at a highly tight cut, there were jet candidates present.

Although this check doesnot certify that the jet is B jet, still the origin of a muon from the center of the dR cone is an interesting observation.All the important parameters used during the study are referred to in Appendix A. The issue for deciding B-jets from jets can be resolved using the pT and the transverse energy resolution. Since the lower threshold for the filter while running it with the trigger simulator was kept at 9 GeV , all jets with a minimum E_T of 9 GeV were selected for the algorithm. A

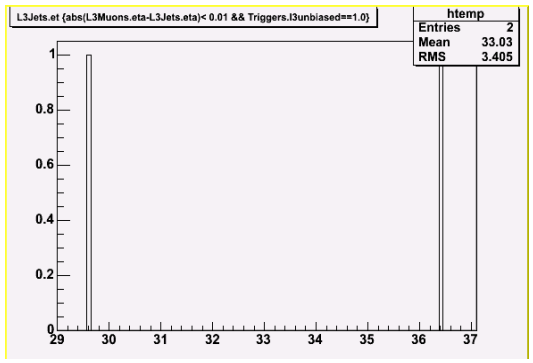

Figure 6.20: The check for 2 jets at dR≤0.01 confirmed by 2 different towers at different η values

scatter plot of jet E_T against η for accepted events show a concentration in the 30 GeV region in the hard section of the detector.

The last row of the table 6.1 suggests that there are 2 jets present with the most stringent match between muon and the jet candidates. The following plot (Figure 6.20) show the 2 jets with their respective E_T distribution. The presence of 2 jets at η=1.0 with E_T 29.64 and at η= -0.6 with E_T=36.4 suggests that the algorithm is accurately checking for all possible candidates in the proper central region of the detector.

6.6 Efficiency

No study is complete without efficiency calculations. Independently, the efficiency has been calculated for both data as well as MC. In a root session, the accepted events have been checked against the accept ratios for various bins of dR. The relationships used are :

$$efficiency = \frac{Passed}{Total} \times 100$$

$$rejection = \frac{Total - Passed}{Total} \times 100$$

Table 6.2: $\delta\eta$ cut against number of jets

Table of events	
$\delta\eta$	Jets Present
3	130
2.5	126
2	123
1.5	116
1	97
0.8	90
0.6	79
0.4	67
0.2	54
0.1	27
0.05	15
0.03	11
0.02	8
0.01	2

6.6.1 Absolute and Differential Efficiencies

It is an interesting observation that although efficiencies can be calculated and interpreted in different ways, the absolute and differential efficiencies provide significant insight of the productivity of the filter. Absolute efficiency is calculated in order to find out the total absolute output rate of the trigger. In this case, the background consists of all events inputed to the trigger and the output is the total events fed to the MarkandPass filter after passing the trigger. The curves are all cumulative in nature and flatten or saturate at a point where the rate of writing events stabilizes with respect to change in dR cut. Another suggested name for this is integral efficiency.

Differential efficiency is calculated for different bins of dR cuts. The dR cut in this case is also applied over the background events. As a result, the output is the efficiency of a partial dR chunk of the data only. Although the absolute efficiency is

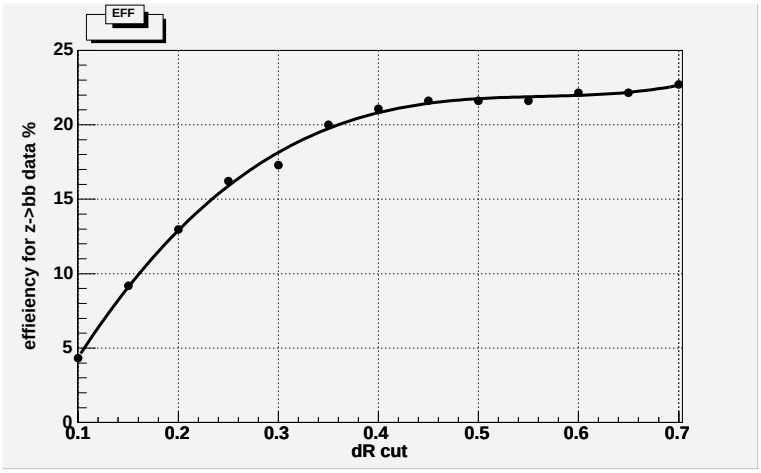

Figure 6.21: The absolute efficiency vs dR cut distribution for MC events

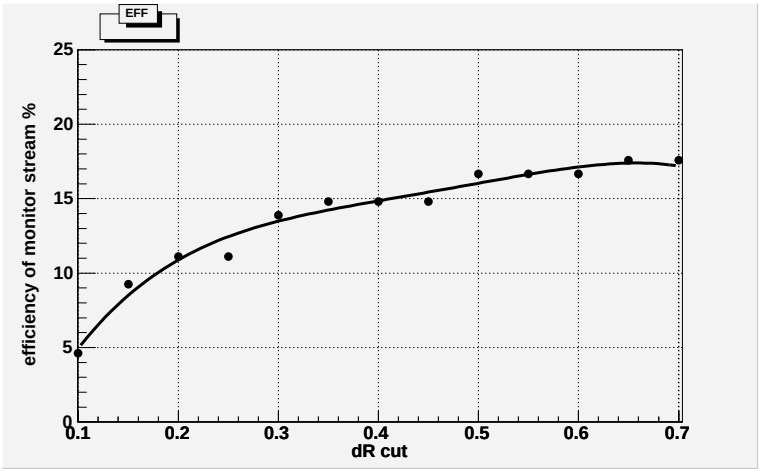

Figure 6.22: The absolute efficiency vs dR cut distribution for monitor stream data

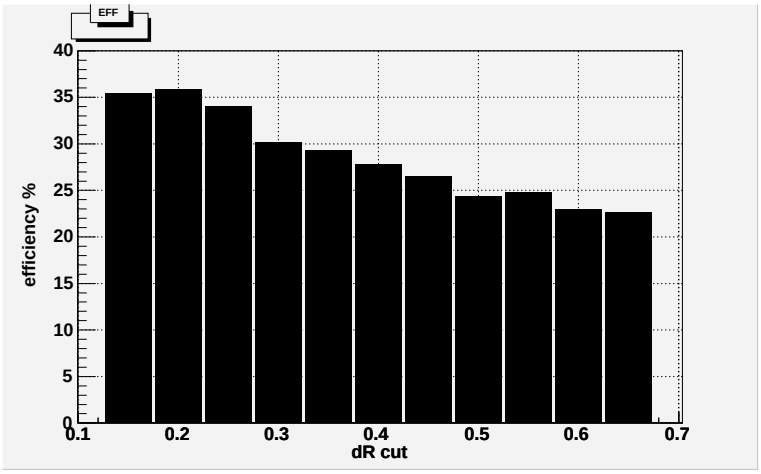

Figure 6.23: The differential efficiency vs dR distribution for MC events

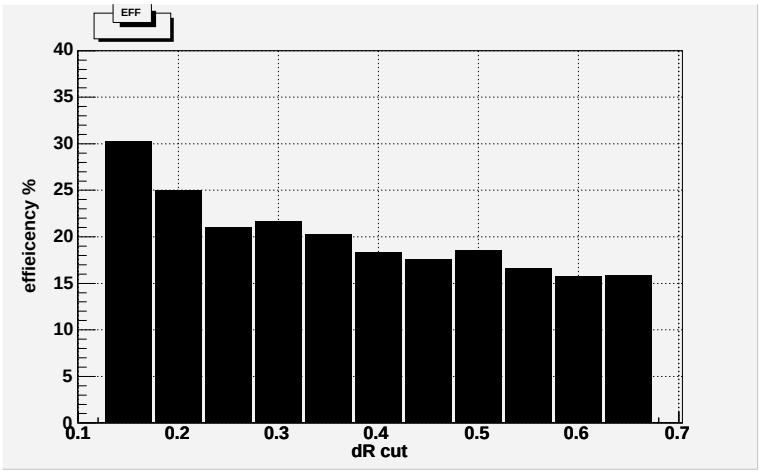

Figure 6.24: The differential efficiency vs dR distribution for monitor stream data

the only interesting plot as long as trigger rates are concerned, maintaining a parallel differential efficiency helps in determining the cuts to be provided to the simulation reference file for higher event resolution.

6.7 Conclusions

The proper quantitative analysis of B-jets and their associated processes paves the way for a better understanding of the Standard Model. For example, the detection of both the top quark and the Higgs boson relies on proper identification and reconstruction of

the B-jets. Due to the low cross-section of the Higgs and top production as compared to the total inelastic, non-diffractive cross section, B-jets assume the role of sensitive probes.

The algorithm developed in the current work provides a handy tool for calculating the efficiency of B-jet tagging at Level-3. When tested on Run II data, the absolute efficiency was found out to be 17.25%. With differential increment of 0.1, in dR the probability of finding a B-tagged event from randomly picked data was found to be 15.68%.

L3FBTagMU is currently running both online and offline through Level-3 triggers.

APPENDIX A

CODE SPECIFICS

A.1 The Level3.sim File Tools

The level3.sim file is a specification file which specifies the configuration of the filters, tools and triggers. Three different tools are mentioned. SCJET9PV1 uses the code L3TJet.cpp from the cvs with parameters specified within brackets. IPTracker is an instance of the L3TIPTracker class with the parameters as mentioned below. Similarly, the muon tool code produces an instance of a specific class.

```
SC5JET_9_PV1 L3TJet(
                calclus=CAL_CLUS5_PV1_NLC_ON,
                algorithm="SC",
                vertex=PrVTX_Z_TRK,
                MinEt=9.,
                MinPreEt=0.,
                ES_R=.8,
                kt_cut=5.,
                tooltype="physics")|

IPTracker L3TIPTracker(
                TRACKER=GlobalTracker,
```

```
                VERTEX=XYVtx05_beam,
                ptcut=.4,
                tooltype="physics")|

MUON_CM L3TMuon(
                tooltype="physics",
                muontrackrefset=MUO_LOCAL,
                centralmatchrefset=MUO_CENTRAL_MATCH,
                muocalmatchrefset=NONE)|
```

A.2 The Level3.sim File Trigger

The specifications of the trigger are mentioned after the tools. They consists of tools, filters, and filter specifications. Each filter is called with a key referring to its respective code either in the central CVS or in a local build executable.

```
L2trig 1^CEM23_19_HTA80|
        filter CEM23_19_HTA80 |
        L3FJet key=t1s2p1_Jet    refset=SC5JET_9_PV1
 number=1 MinEt=9. MinEta=0. MaxEta=3.6 Stream="ALL" |
        L3FIP key=t1s2p2_IP      refset=IPTracker number=1
 MinIP=1.0 MaxIP=20. MinPt=0.5 MinXYHits=10 MinZHits=0
        MinSMTXYHits=2 MinSMTZHits=0 Stream="ALL" |
        L3FMuon key=t1s2p3_Muon  refset=MUON_CM number=1
MinEt=0. MinEta=0. MaxEta=4.0 MinPhi=0. MaxPhi=6.29
        MinPtLocal=0. MinPtCentr=0. MinQuality=LOOSE
 CalMatchReq=FALSE CentralMatchReq=TRUE Stream="ALL" |
        L3FBTag_MU  key=t2s2p4_BTag_MU jetfilter=t1s2p1_Jet
 muonfilter=t1s2p3_Muon ipfilter=t1s2p2_IP DR=0.7
```

```
        jet_et_cut=9. Stream="ALL" |
 L3FMarkAndPass key=t14s1_mp1     pass_1_of_n=1. Stream="ALL" |
 ||
```

A.3 The Filter.rcp File

The filter.rcp file is needed in order to specify the filter's parameters. The numbers written after the parameters are the default values followed by the minimum and maximum in order.

```
**********
L3FBTag_MU
key
muonfilter
ipfilter
jetfilter
jet_et_cut     15.0   8.0   25.0
DR              0.5   0.1    0.7
Stream         "NULL"
*********
```

APPENDIX B

PRESENTATIONS

The following are links to presentations enroute to the development of the trigger and service work with the STT group as an expert.

B.1 For Level-3

November 25, 2003, Introduction to the Trigger Framework of Level 3

`http://www-d0.hef.kun.nl///askArchive.php?base=agenda&categ=a03624&id=a03624s1t54/transparencies`

June 22 , 2004, Proposal to Level-3 , algorithm group for the new code

`http://www-d0.hef.kun.nl///fullAgenda.php?ida=a041042`

August 31, 2004, Plan on the specifics of the Design to Level 3 Algorithms

`http://www-d0.hef.kun.nl///fullAgenda.php?ida=a041448`

October 12, 2004, Report to the DØ Collaboration Meeting about initial studies

`http://www-d0.hef.kun.nl///askArchive.php?base=agenda&categ=a041583&id=a041583s1t69/transparencies`

November 9, 2004: Initial efficiency studies with restricted parameters for L3FBTagMU

http://www-d0.hef.kun.nl///askArchive.php?base=agenda&categ=a041864&id=a041864s1t69/transparencies

November 19, 2004. Submission of code to the L3 Algorithm group.

http://www-d0.hef.kun.nl///askArchive.php?base=agenda&categ=a041921&id=a041921s1t13/transparencies

December 8, 2004: DØ Collaboration Meeting talk on Online/Offline comparison for P17.04.00 data

http://www-d0.hef.kun.nl///fullAgenda.php?ida=a042037

March 29, 2005: Final submission of efficiency study for L3FBTagMU filter.

http://www-d0.hef.kun.nl///askArchive.php?base=agenda&categ=a05562&id=a05562s1t8/transparencies

B.2 Expert Panel Reports for Silicon Track Trigger

December 27, 2004, STT expert report for the week.

http://www-d0.hef.kun.nl///fullAgenda.php?ida=a042124

January 10, 2005 , STT expert report for the week.

http://www-d0.hef.kun.nl///fullAgenda.php?ida=a0532

February 21, 2005, STT expert Summary for the week.

http://www-d0.hef.kun.nl///fullAgenda.php?ida=a05277

March 14, 2005, STT expert Summary for the week.

http://www-d0.hef.kun.nl///fullAgenda.php?ida=a05436

March 21, 2005, Special report over month's statistics.

http://www-d0.hef.kun.nl///fullAgenda.php?ida=a05472

BIBLIOGRAPHY

[1] B. Balding. Global track finding at level 3. D0 Note 3808, 2002.

[2] P. Balm. Central track matching of muon tracks at level 3. D0 Note 3934, 2002.

[3] P. Balm, C. Clement, H.T. Diehl, M. Mulders, S. Soldner-Rembold, and M. Wegner. The d0 level 3 muon filter. D0 Note 3999, 2002.

[4] R. Bernarhd. Search for rare leptonic b decays at the tevatron. D0 Note 4645, 2004.

[5] D0 Collaboration. D0 run iib silicon detector, technical design report. D0 Internal Report, 2003.

[6] D0 Collaboration. Search for neutral supersymmetric higgs bosons in multi-jet events at sqrt(s)= 1.96 tev. D0 Note 4718, 2005.

[7] High Energy Physics Community DOE/NSF. Einstein's unified force theory. *Quantum Universe*, I:26–39, 2004.

[8] H. Dong. An impact parameter for the d0 experiment. D0 Note (Internal),submitted to IEEE, 2003.

[9] S. Fatakia. *A Measurement of the Mass of the Top Quark in the Di-LEpton Channels using the DØ Detector at Fermilab*. PhD thesis, Boston University, 2005.

[10] D. Griffiths. *Introduction to Elementary Particles*. John Wiley and Sons, 1987.

[11] D Griffiths. *An Introduction to Quantum Electrodynamics*. John WIley and Sons, 1987.

[12] L. Gunion, H.E. Haber, G.L. Kane, and S. Dawson. *Higgs Hunters Guide*. Addison Wesley, Redwood City, CA, 1990.

[13] A.C. Haas. *A Search for Neutral Higgs Boson at High tan β in Multi-jet event from ppbar Collisions at sqrt(s) = 1960 GeV*. PhD thesis, University of Washington, 2004.

[14] S. Hope. Jet algorithms. Jet Seminar, University of Bonn, 2004.

[15] H. Kim, J. Yu, D. Meyer, M. Sosebee, P. Bhamidipati, and K. Gopalratnan. Understanding the mcfarm, uta's linux-farm controller for d0 mc generation. D0 Note 4414, 2003.

[16] B. Lee. Daq shifter tutorials. D0 Shifter Documentations, Internal, 2004.

[17] L.B. Okun. *Alpa Beta Gamma .... Zeta, A Primer in Particle Physics*. Cambridge University Press, 1987.

[18] O. Peters. Muon segment reconstruction. D0 Note 3901, 2001.

[19] O. Peters. Measurement of b-quark content in jets with pre-shutdown data. D0 Note (Internal), 2002.

[20] O. Peters. *Measurement of the b-jet cross section at sqrt(s)=1.96 TeV*. PhD thesis, Universiteit van Amsterdam, 2003.

[21] TriggerMeisters. Trigsim cookbook and manual. D0 Internal documents, 2002.

[22] B. Wijngardeen and F. Filthaut. Impact parameter tracking. D0 Note 3850, 2001.